JAERI 1035

Corrosion of Alminum in Water

1963年3月

日本原子力研究所

Japan Atomic Energy Research Institute

UDC: 620. 193, 669. 71

Corrosion of Aluminum in Water

Summary

(1) A large amount of aluminum and its alloys being used in flowing water at temperatures below 100°C in the JRR-2 and JRR-3*, dynamic corrosion of aluminum was studied under conditions corresponding to those prevailing in reactors.

When commercial grade pure aluminum is corroded in flowing water at 50°C~70°C, the weight of the aluminum specimen will increase with time at low flow rates, and decrease with increasing flow rate. The change of weight of the specimen is also affected by water purity and conditions of surrounding atmosphere.

The total amount of corrosion from chemical analysis does not always parallel the change of weight of the specimen, and pitting (about 10 microns in diameter) is also observed to occur in many specimens. It can therefore be concluded that it is difficult to estimate the corrosion amount only from the change of weight of the specimen.

In several cases the relation between the properties of surface oxide film and corrosion reaction in flowing water was established.

(2) With the further objective of developing aluminum alloys that are corrosion-resistant in hot water, some studies on the corrosion mechanism of aluminum alloys in hot water and steam were conducted.

In hot water, aluminum is corroded easily with higher purities of the metal, and according to DRALEY, this is due to the penetration of hydrogen into the grain boundaries. Various methods were used to ascertain his mechanism, and in particular, hydrogen evolution at the grain boundaries was directly observed in a windowed autoclave.

It was also established by X-ray and electron-microscopic methods that the transformation and structual change of the surface oxide film modifies the kinetics of corrosion of alminum in steam around 350°C.

June, 1962

M. KAWASAKI, S. NOMURA, H. ITAMI, Y. KONDO,
T. KONDO, N. ITO and C. AKUTSU
Metallurgical laboratory
Japan Atomic Energy Research Institute

* Japan Research Reactor-2, Japan Research Reactor-3.

アルミニウムの腐食

総　　括

1. 静止純水中における腐食　50°C～90°C の温度範囲における静止純水中 99.99% Al の腐食に関する動力学的研究ならびに腐食生成物としての表面被膜の構造解析がおこなわれた．80°C 以下では，反応は三段階を経て進行し，反応速度は第一，第二段階では大きく，第三段階ではほとんど無視できるほど小さい．第一段階では，対数則に従って，boehmite のうすい被膜が生長する．反応速度恒数は温度とともに減少し，これによって，反応の活性化エネルギーは，$\Delta H = -4.1$ kcal/mole と計算された．Boehmite 被膜は二重構造をなしており，外側の被膜は通常の boehmite，被膜の大部分を占める擬 boehmite が内層として存在することが明らかとなった．第二段階ではこの boehmite 被膜上に bayerite 結晶が析出し，同じく対数則に従って膜状の発達をなし，ついには完全に表面をおおうに至る．同時に反応は，第三段階に移り，腐食反応はほとんど抑制される．90°C では，第一段階における boehmite 被膜は，均一構造をもち，通常の boehmite から構成されている．その成長は放物線則に従い，約 100 時間にわたって第一段階が継続する．第二段階において生成される bayerite 結晶は，三次元的な成長をおこない，また初期に形成された結晶の成長が優先するために膜状の発達がおさえられ，200 時間経過後も bayerite が全面をおおうに至らなかった．

2. 原子炉被覆材として使用される 1100 Al 合金の流動　水中での腐食挙動を，(i) 流速の影響，(ii) 水質および添加ガスの影響，(iii) 表面被膜処理の影響について検討した．

(i) 流速の影響：70°C の高純度水（比抵抗 1 MΩ-cm 以上）中で，0.07 m/sec の低流速では，重量増加 3 m/sec，6 m/sec の高流速では重量減少となり，見かけ腐食速度と流速との間に $|R| \propto V$ (R; 見かけ腐食速度，V; 流速）の関係式が得られた．また表面観察の結果，各流速とも数 10 μ 径の pitting が見られ，高流速では groove 状になることが観察された．

(ii) 水質および添加ガスの影響：70°C, 3 m/sec の流動水中でイオン交換樹脂で水質と制御した場合，精製水では，重量減少，非精製水では重量増加となり腐食速度は前者は後者に比較して 5 倍以上も大きく，腐食速度は Al の溶解速度によって支配されることがわかった．また，非精製，精製水の両者について，H_2, O_2 ガスを 70°C で溶解させて，添加ガスの影響を検討した結果，溶解ガスをともなう場合は，非精製，精製水ともに重量減少となり，とくに H_2 添加の精製水では重量減少が著しかった．しかし，腐食速度は添加ガスの場合，非精製，精製水にかかわらず，腐食速度にあまり差が認められなかった．また，腐食挙動と腐食生成被膜中の barrier film の厚みの関係を検討した結果，Al の水中への溶解しやすさと barrier film との間に密接な関係があることが認められた．また，O_2 添加ガスの非精製水中では，電気化学的な galvanic action による Al の腐食が観察された．

(iii) 表面被膜処理の影響：化学研磨，bayerite 被膜処理，boehmite 被膜処理した試料について表面処理の影響を検討した結果，化学研磨 Al は 50°C, 70°C, 1.5 m/sec の条件でともに重量増加となり，50°C の場合は腐食生成物（bayerite 被膜）の生成速度と腐食速度と密接な関係が認められた．しかし，70°C ではこの関係が認められなかった．Bayerite 被膜処理した Al 70°C, 1.5 m/sec, 2.5 m/sec の条件でともに重量増加となり，boehmite 被膜処理した Al は，同一条件でわずかに重量減少を示し，表面の被膜処理と腐食挙動と密接な関係があることがわかった．

3. 高温静止水中における腐食　100°C から 250°C まで高温静止水中での Al の腐食に及ぼす腐食環境および金属組織の効果を研究した．とくに 100°C 以上の高温水中での腐食において問題となる粒界腐食の機構解明に重点をおいている．一般に Al の純度が下がるにしたがって，粒界侵入および全面腐食は減少し 99% Al では粒界腐食は起こらない．99.99% Al の結晶粒度を，strain-annealing 法によって種々に変えたが，粒界侵入深さは粒の大きさに響影を受けなかったが全腐食量は粒の大小によって左右される．これは多分結晶

粒界の密度に関連があると考えられる．少量の KOH または H_2SO_4 を加えて，水の pH を調節した場合，pH 3 の付近でもっとも腐食量は小さく，また粒界腐食もほとんど抑制される．pH 3 を境として pH の低い領域では腐食による重量減少がみられる．強加工をほどこした 99.99% Al はほとんど粒界侵入を受けないが表面被膜の結晶化が促進され被膜の脱落が著しくなる．この場合加工によって生じたすべり集合体もまた粒界と同じように選択的に腐食される．99.99% Al を基として種々の添加元素を加えて二元素合金を作り，耐食性の比較がおこなわれた．銅を除く Al より貴な元素を加えた場合，表面被膜の結晶化にもとづく，試料の崩壊までの誘導時間が著しく延長され，なかでも Ni 合金がとくにすぐれた性質を表わした．反対に卑な元素を加えた場合は，逆の結果が起こると同時に粒界侵入もはげしくなる．水素，アルゴン，酸素ガスを系内に導入した際には，この順序で腐食は増加するが逆に粒界侵入は減少する．のぞき窓付オートクレーブを用いて粒界侵入の模様を観察したが，侵入に先だって水素気泡が粒界より生成されることが明らかとなった．

4. 高温高圧水蒸気中の腐食 高温の飽和水蒸気および過熱水蒸気中の Al の腐食について動力学とそれに並行する生成酸化物の解析がおこなわれた．腐食の動力学的な挙動は 320°C～350°C を境として変り，生成する酸化被膜も著しい相違を示す．210°C から 320°C に至る範囲での飽和水蒸気による腐食は paraboric な時間依存性の速度則によって進行し，生成酸化被膜は一水化物の boehmite であった．反応の速度恒数から計算された活性化エネルギーは 32 kcal/mole の低い値を示し，無水 Al 酸化物の水和が腐食反応を支配していることが推定された．一方 350°C および 400°C での過熱水蒸気中の腐食はきわめて腐食量が少なく測定値は無視できるほど小さかったが，圧力依存性が $p^4 \propto t_i$ なる関係の誘導期間をもった急速で無秩序な貫通性の局部腐食が観察された．この高温領域での生成酸化被膜はきわめてうすく，かつちみつで，部分的にαアルミナ結晶を含んだ非晶質被膜であることが電子顕微鏡および電子回折によって確認され，さらに貫通性腐食の原因は被膜内側に生成し，金属中に吸収されて結晶粒界に集積した水素ガスによるものであることが明らかにされた．

1962年6月

原子力工学部金属研究室
川崎正之，野村末雄，伊丹宏治
近藤達男，近藤靖子，伊藤　昇
坪　　長

Contents

目　　次

INTRODUCTION

Two of the three reseach reactors at JAERI consist of a core tank and aluminum clading fuel elements which is in contact with D_2O as the coolant or moderator. Although the corrosion of 1100 alminum seems to induce no trouble under ordinary conditions below 100°C, there is no doubt that information needs to be obtained of the corrosion behaviors under the conditions similar to those in the reactors. The several works reported in chapter 1 have been carried out at JAERI, supplementing the comprehensive work[1] on corrosion of aluminum in water held by Japan Institute of Light Metals.

The low thermal neutron absorption and low price of alminum may be very attractive if it can be used in the high temperature water condition. For this reason numerous works have long been performed to develop corrosion-resistant aluminum alloys in high temperature water. The development of X 8001 alloy is one of the results from those works. However the mechanism and reaction kinetics of corrosion of aluminum in high temperature water and steam have not been clearly established, and so several experiments reported in chapter 2 were carried out to make them clear, especially in the case of steam corrosion.

1 CORROSION BELOW 100°C

1.1 Static Corrosion Test

1.1.1 Experimental

A. Materials: Rectangular coupons of 99.99% aluminum (80×40×1 mm) were cut from a rolled sheet of aluminum and then annealed in a vacuum furnace at 400°C for 1.5 hours. They were chemically polished in a H_3PO_4+10% HNO_3 solution at 85°C for 2 minutes to remove the surface layer formed when mechanically shaped. Then they were rinsed sufficiently with distilled water.

After degreasing, they were dried in a desiccator by pumping for 1 hour and weighed within the accuracy of 0.1 mg.

B. Test Condition: The water used was prepared by distillation followed by deionization through a mixed-bed ion-exchanger. The specific resistance of the purified water became more than 5 MΩ-cm at room temperature.

Prior to the immersion of specimens, the water was preheated for 24 hours in a sealed 500 m*l* polyethylene bottle placed in an air-bath thermostatically maintained at the test temperature within the accuracy of 0.3°C. This preheating process was intended to attain an equilibrium oxygen content with water at the

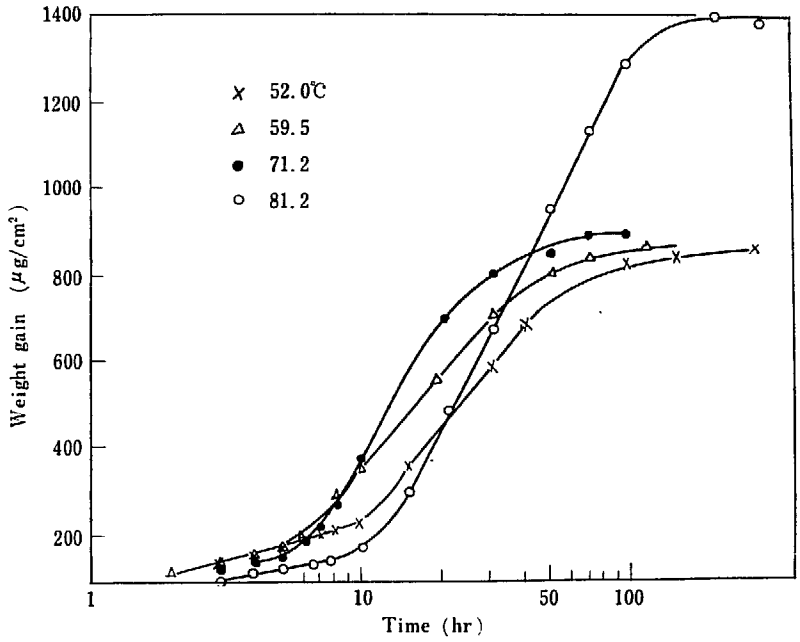

Fig. 1 Relation between weight increase and logarithmic time

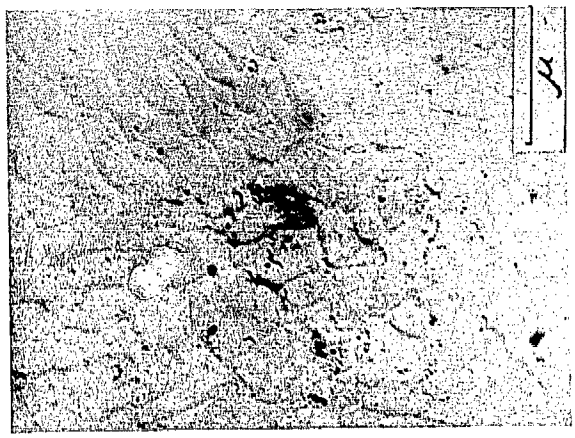

a) 30 min
A random nucleation starts.

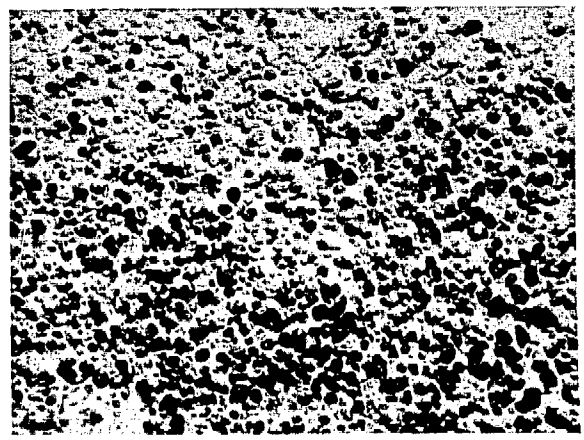

b) 40 min
The surface is covered with nuclei.

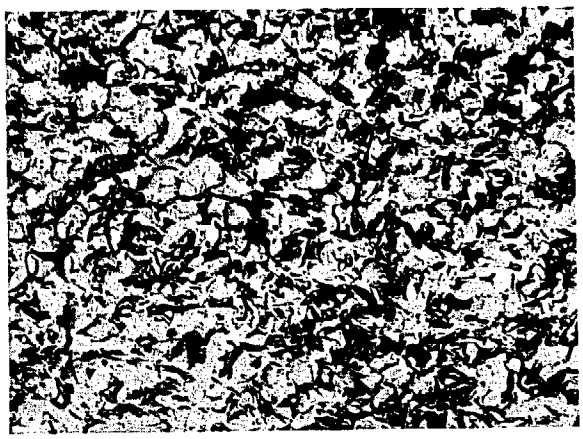

c) 120 min
The crystals are glowing.

Fig. 2 The nucleation and growth of boehmite crystals at 70°C

test tepmerature. The water was replaced with the fresh one every 24 hours during the test and the dissolved aluminum was quantitatively analyzed.

The corrosion tests were carried out at 50°C to 90°C. After each removal of the specimen, it was dried in the vacuum desiccator for 1 hour and reweighed.

The surface corrosion product of the specimen was examined with optical and electron-microscopes, and identified by X-ray and electron diffraction methods.

1.1.2 Results and Discussion

The weight change against logarithmic time at 50°C to 80°C is shown in Fig. 1, each plot being the average of 4 specimens (total surface area, 256 cm^2). From these curves it is found that the corrosion process takes place in 4 steps in this temperature range.

The corrosion product at the first stage was determined by HART[2] to be crystalline-boehmite, and DRALEY[3] suggested that the growth of the protective boehmite film was logarithmic. In the present study, at 70°C for example, it was observed that a random nucleation of very fine spherical crystals occured on the specimen (Fig. 2b) when immersed for 30 minutes; then the surface was covered with the nuclei the 10 minutes after (Fig. 2b). They grew up for 2 hours after the start of

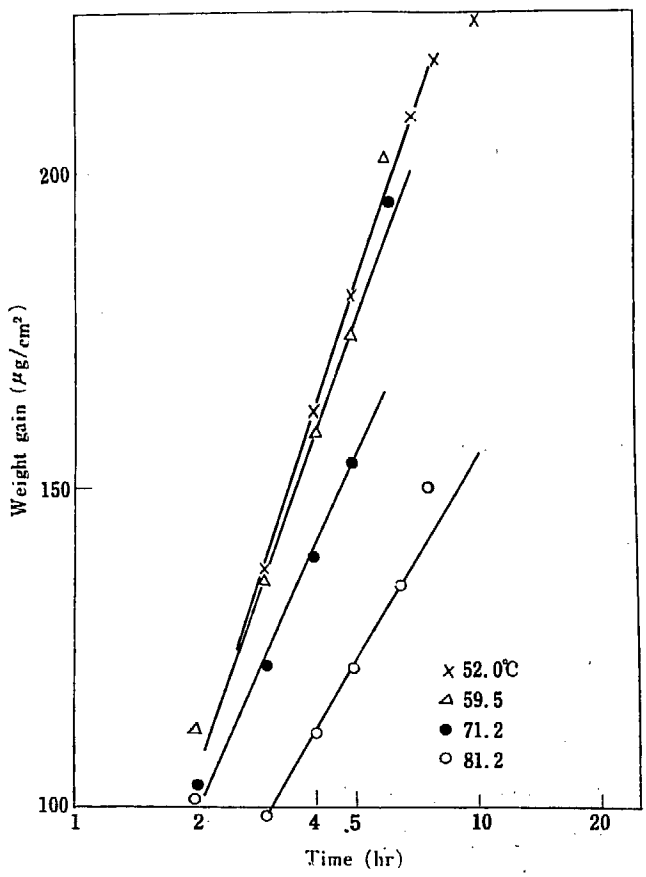

Fig. 3 Relation between weight increase and logarithmic time in the first stage

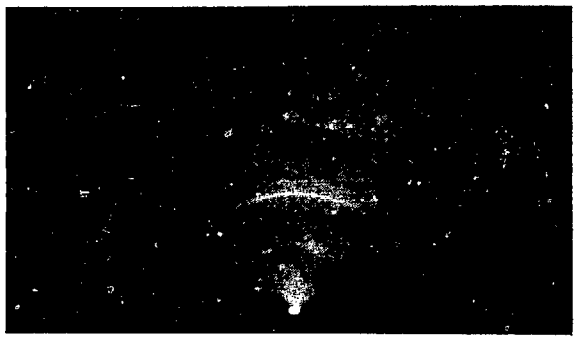

a) Boehmite (70°C, 2 hr)

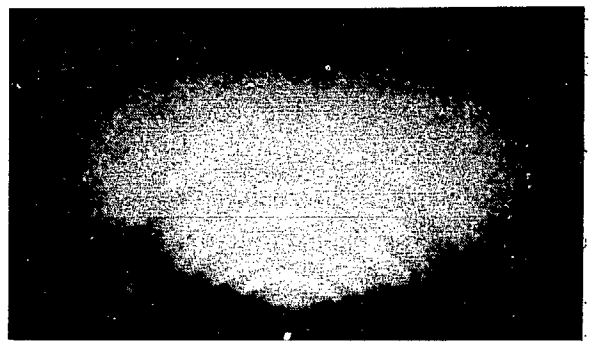

b) Boehmite (90°C, 2 hr)

c) Bayerite single crystal (70°C, 100 hr)

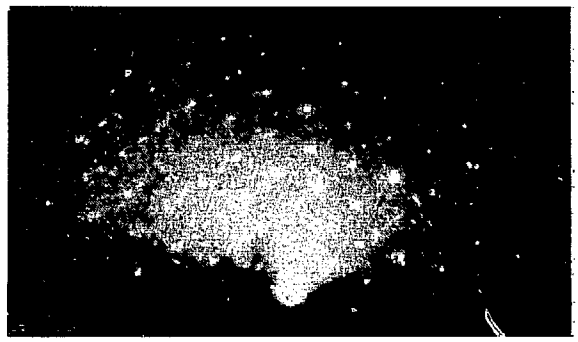

d) Bayerite single crystal (90°C, 100 hr)

Fig. 4 Electron diffraction patterns of surface oxide

immersion, as shown in Fig. 2c).

Figure 3 shows that the reaction in the first stage follows the logarithmic rate law, it agrees with the DRALEY's result. It is found that the process of the film growth is accord with the CABRERA-MOTT's theory on the logarithmic growth-rate law for very thin oxide film[4], as the thickness of the present oxide layer is determined to be less than 100 Å. The surface film in this stage was identified with boehmite by the surface electron diffraction, as shown in Fig. 4a).

After four hours of immersion, different kind of large crystals appeared on the surface of boehmite (Fig. 6a).

The deviation of the curves from the first logarithmic parts (Fig. 1) is due to the crystalization of bayerite on the surface of boehmite. Thus the beginning of this is considered to be the end of the first stage in the kinetic process.

It was also found that a slight intergranular attack occured, as shown in Fig. 5c), d) which did not proceed with immersion time beyond a certain point but proceeded with increasing the temperature in the present experiment. Thus it is thought that there exists relation between the intergranular attack and the boehmite formation, because the elimination of the proceeding of the attack and the bayerite formation were almost simultaneous, whereas the intergranular attack continued as shown in Fig. 5a), b) at 90°C where the formation of boehmite was most predominant.

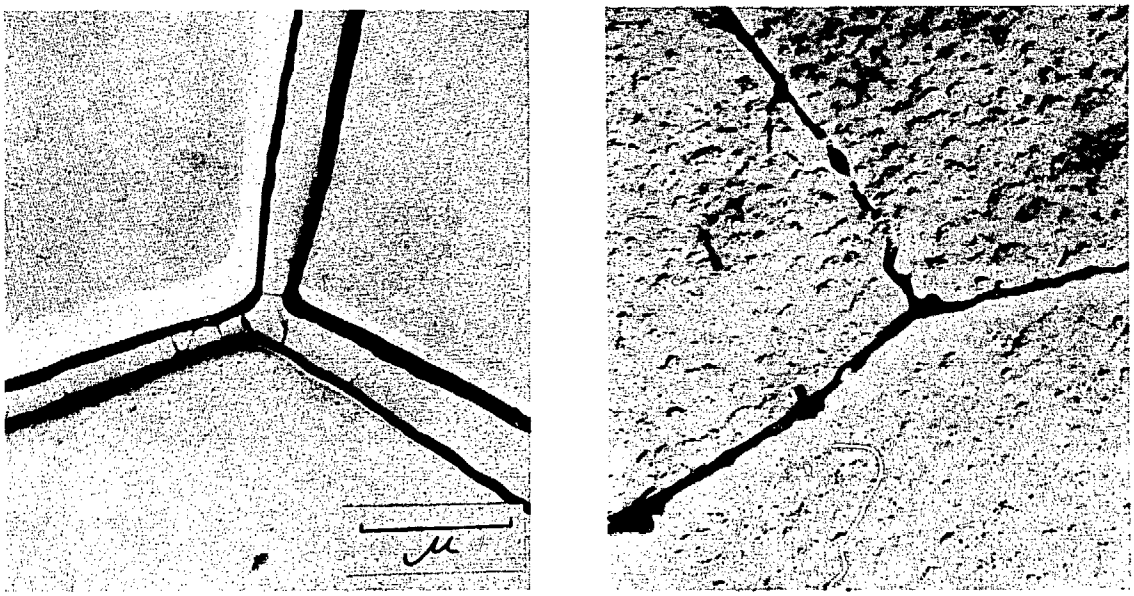

a) c)

Electron-micrograph

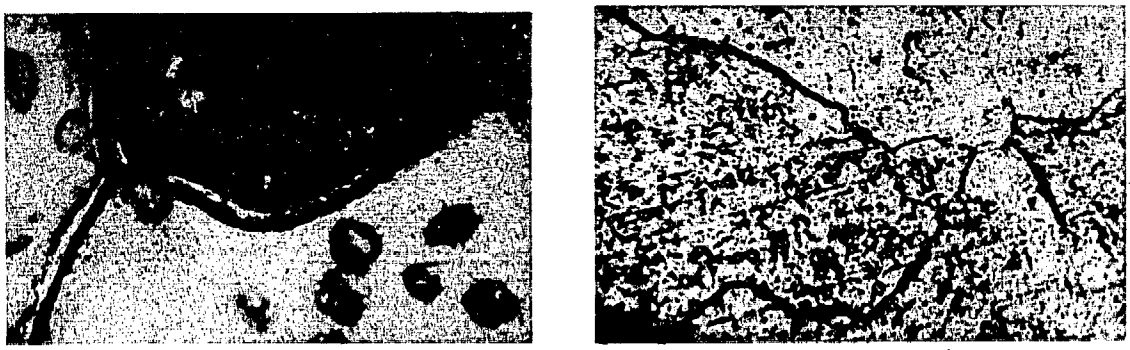

b) (90°C, 20 hr) d) (50°C, 20 hr)

Optical-micrograph

Fig. 5 Intergranular corrosion of 99.99% aluminum in water
(a, c: defilmed surface)

The second stage started with the appearance of bayerite crystals on the boehmite of the first stage and the weight gain became suddenly large, as shown in Fig. 1;

The logarithmic rate law is represented as

$$\Delta W = k_1 \log (t - \alpha_1), \qquad (1)$$

where ΔW is weight change, α_1 varies with temperature, and the value of k_1 is 490 μg/hr·cm^2. The most interesting feature of k_1 is the temperature independence, and the following relation between the reciprocal temperature and the logarithm α_1 corresponding to the induction time for the appearance of the new crystals was obtained as

$$\ln \alpha_1 = -\Delta H_1/RT + \ln A_1, \qquad (2)$$

where ΔH_1 was calculated to be 4.1 kcal/mole as shown in Fig. 7.

The new crystals were determined to be bayerite ($Al_2O_3 \cdot 3H_2O$) by X-ray and

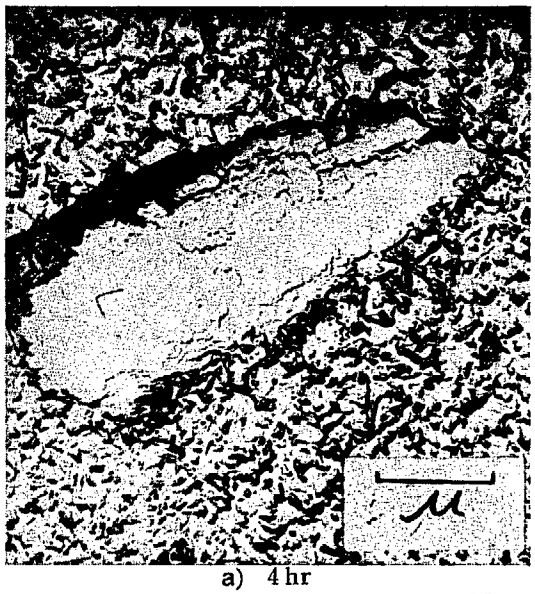

a) 4 hr

b) 20 hr

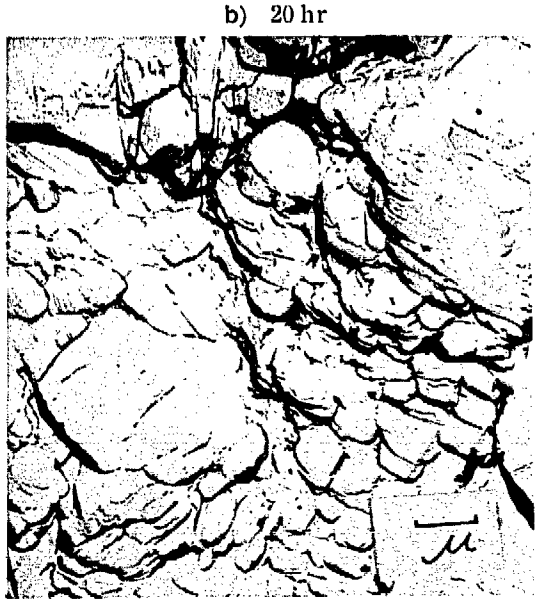

c) 100 hr

Fig. 6 Growth of bayerite crystals on the boehmite film at 70°C

a), b) and c): electron micrographs
b′) and c′) : optical micrographs surface replica ×40

b′)

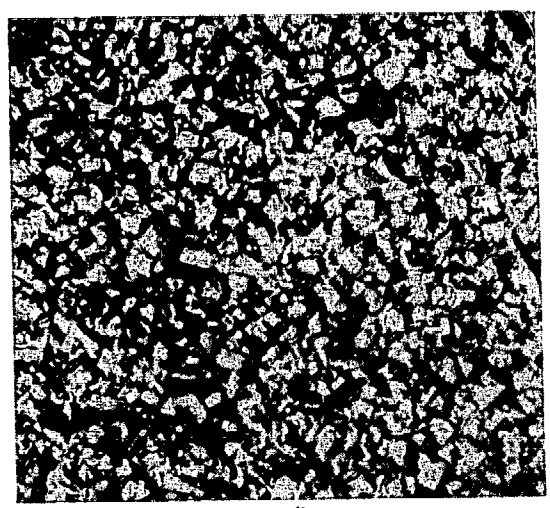

c′)

electron diffractions (Fig. 4) and grew up three-dimensionally with time, as seen in Fig. 6a), b) and c). Several interpretations have been proposed for the mechanism of the development of such bayerite crystals, two of which are the dissolution-precipitation[5] and the breakaway hypotheses[3] based on the hydration of boehmite. The authors favor the precipitation process since the solubility of boehmite in water is ten times larger than bayerite and the latter is thought to be more stable than the former in this temperature range. Moreover, the activation energy for the crystallization calculated from the equation (2), is much closer to that for oxide dissolution, calculated by SAKAMOTO[6] to be 3.74 kcal/mole. Thus it is thought that the nucleation-growth process corresponds to the precipitation which was induced by the large difference of solubility between the two kinds of hydrated aluminum oxides.

It is note-worthy that the amount of dissolved aluminum was determined as 8.5×10^{-7} grams/mole at 50°C by chemical analysis in the second stage, where both oxides were exposed to water; this value is approximately the intermediate of the solubilities of both oxides. The solubility of boehmite was calculated to be 6×10^{-6} grams/mole using the solubility product[7]. When the whole surface was covered with bayerite the dissolved aluminum was determined to be less than 1.7×10^{-7} grams/mole, which agrees with the solubility of bayerite, 1.5×10^{-7} grams/mole determined by FRICHE and MEYRING[7].

When the process moved to the third stage the reaction rate decreased drastically but followed the logarithmic rate law represented by

$$\Delta W=k_2 \log (t-\alpha_2)+\log \Delta W_1, \qquad (3)$$

where $\alpha_2=7$ (hr) and $\Delta W_1=786$ (μg/cm^2)

A logarithmic plot of k_2 against the reciprocal temperature is shown in Fig. 7 and generally

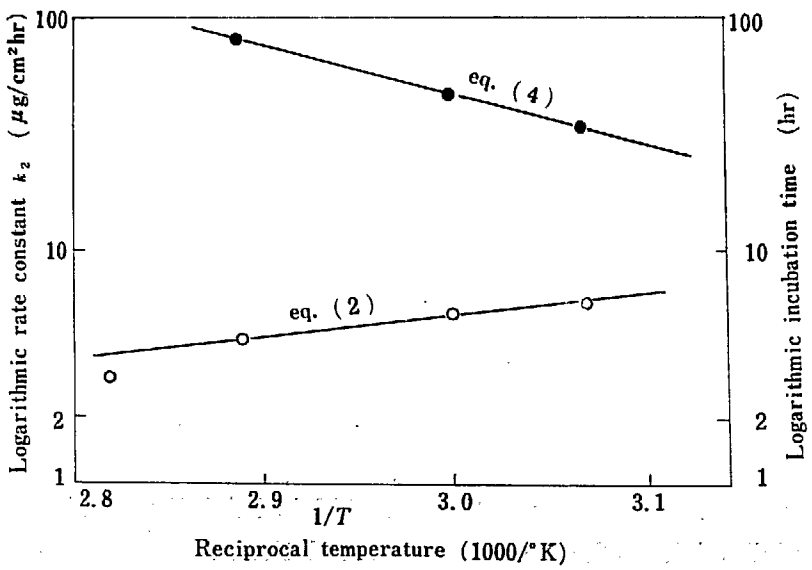

Fig. 7 Effect of temperature on logarithmic constants of corrosion

$$k_2 = A_2 \exp(-\Delta H_2/RT) \qquad (4)$$

Then the activation energy ΔH on the equation (4) is calculated to be $\Delta H_2 = 8.4$ kcal/mole.

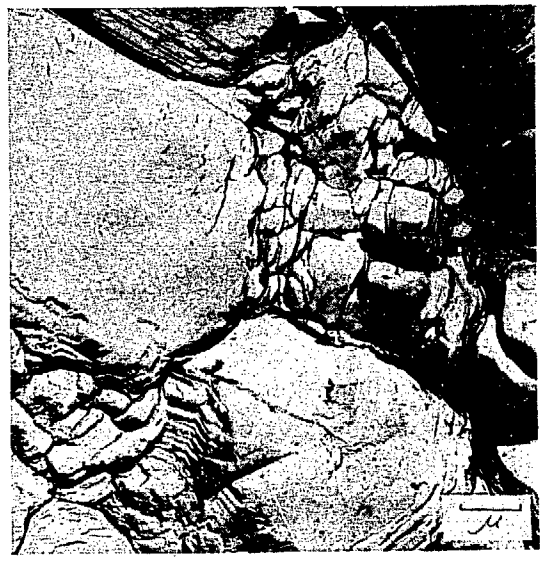

Fig. 8 Crack formation in bayerite crystals at the fourth stage

At the end of this stage there were observed some cracks on the surface of bayerite crystals, as shown in Fig. 8, their origin was, however, not clearly understood yet. Generally the third stage was very short and was followed by the fourth stage. The fourth stage is not discussed because of the lack of data.

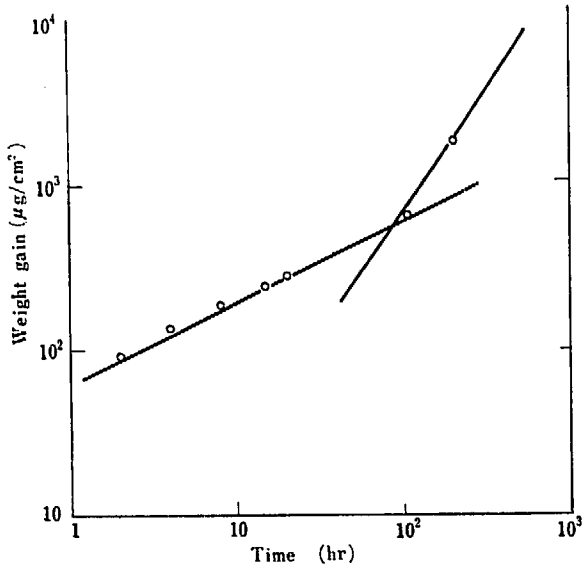

Fig. 9 Relation between weight increase and time at 90°C

It is seen in Fig. 9 that the reaction at 90°C is initially paraboric against time being accompanied with boehmite formation and then moves to a faster stage.

In addition, it is seen that the electron diffraction pattern in Fig. 4 shows the

bayerite single crystals in the latter stage. It is thought to be due to the unfavorite condition for the nucleation of bayerite.

1.2 Dynamic Corrosion Test

1.2.1 Materials

All specimens, 20×50×1 mm, were cut from 1 mm sheets of 1100 aluminum from the same batch, and used in the following three programmes (cf. 1.2.3). In Programme I, the specimens were degreased before test to simulate the metal in the reactor. In Programme II, the annealed specimens were pickled in a 10% NaOH solution and rinsed with demineralized water, and in Programme III, they were chemically polished in a H_3PO_4-HNO_3 solution to obtain the flat surface. It was found by the comparison test that the three kinds of specimens used in the above three programmes showed the similar corrosion behaviors except the initial amounts of corrosion. In Programme III, the prefilmed specimens of bayerite and boehmite produced by immersion in demineralizied water at 70°C and 150°C for 50 hours respectively were also used.

1.2.2 Test Conditions

Three loops, L-1, -2 and -3, were employed for each programme respectively. The L-1 and L-2 loops were mainly made of stainless steel except the gun-metal valves, but the L-3 loop was made of polyethylene except the canned stainless steel pump in order to prevent the introduction of impurity ions from loop components into loop water.

All loops had a bypass-system consisting of a cooler and ion-exchange column to maintain the specific resistance of water in the main circuit above 1 MΩ-cm.

In Programmes I and II, specimens were taken out of the test sections intermittently for weighing and then placed back in the original positions; the amount of metal corroded was measured by stripping off the surface film in H_3PO_4-Cr_2O_3 solution. In Programme III, a quarter of all the specimens were taken out from the test section at each period and were replaced by two kinds of prefilmed specimens obtained by the method described at the end of 1.2.1.

1.2.3 Variables Studied

A. Effect of Flow Rate (Programme I) Four specimens were inserted into each of the three test sections placed along the main circuit of L-1 loop with 0.07, 3.0 and 6.0 m/sec of flow rates respectively.

B. Effect of the Gas Supplied (Programme II) Tests were carried out in water at 70°C and 3 m/sec of flow rate into which hydrogen or oxygen was continuously introduced into the L-2 loop by bubbling.

C. Effect of Water Purity (Programme II) This test was carried out simultaneously with the above tests by the L-2 loop either with or without the bypass purification system.

D. Effect of Surface Oxide Film (Programme III) The corrosion behaviors of the three kinds of specimens, i.e., chemically polished, bayerite and boehmite prefilmed, were compared in demineralized water with flow rates of 1.5 and 2.5 m/sec at 70°C.

The chemically polished specimens were also corroded at 50°C and 1.5 m/sec. The test conditions employed are summarized and listed in the Table below:

Programme	I	II	III
Loop used / Test condition	L-1	L-2	L-3
Surface treatment	As rolled	Pickled in 10% NaOH sol.	Chemically polished Bayerite prefilmed Boehmite prefilmed
Temperature	70°C	70°C	50°C 70°C
Flow rate	0.07 m/sec 3.0 m/sec 6.0 m/sec	3.0 m/sec	1.5 m/sec 2.5 m/sec
Gas supplied	non	non H_2 O_2	non
Water condition	refreshed	refreshed, non-refreshed	refreshed

1.2.4 Results and Discussion

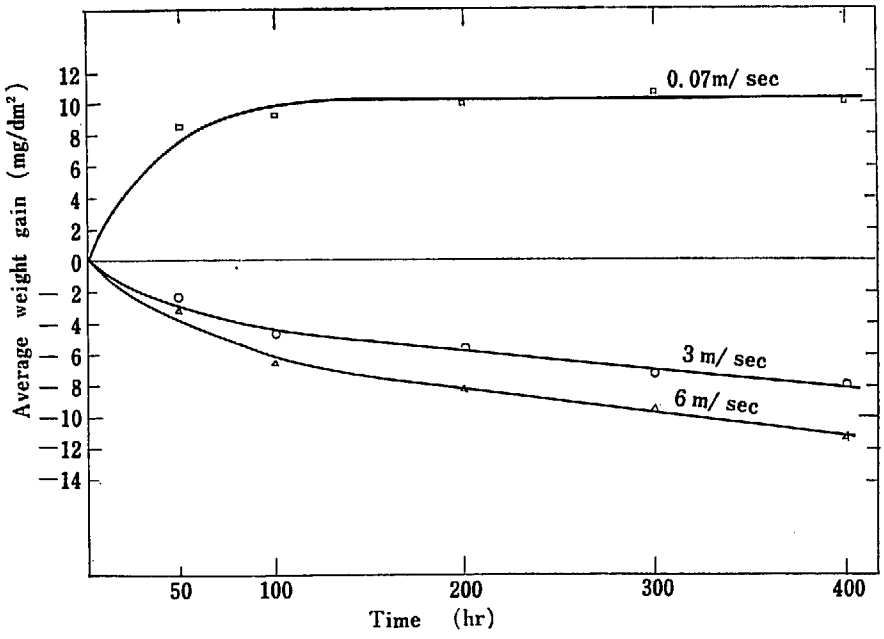

Fig. 10 Weight change of 1100 Al in flowing water at 70°C

A. Programme I The weight changes of the specimens are plotted against time in Fig. 10 which shows the increase in weight at a low flow rate and the decrease at high flow rates.

The amounts of metal corroded, dissolved into water and remaining in the surface film after 400 hours of immersion were measured and calculated by descaling the surface oxide film. The results are summarized in TABLE 1 with the apparent corrosion rate. The apparent corrosion rate was estimated from the weight change between 200 and 400 hours, assuming that a good proportionality between the rates of weight change and corrosion was maintained in the stationary state as it was seen beyond 100 or 200 hours in Fig. 10.

TABLE 1 Results of corrosion test on 1100 Al in flowing water at 70°C.

Velocity	Al in surface film (mg/dm^2)*	Al dissolved (mg/dm^2)	Total Al corroded (mg/dm^2)	Apparent corrosion rate (m. d. d.)
0.07 m/sec	7.99	5.40	13.39	+0.04
3 m/sec	18.62	42.75	61.37	−0.27
6 m/sec	20.65	47.63	67.74	−0.37

* The composition of surface film was estimated as $Al_2O_3 \cdot 3H_2O$ from chemical analysis.

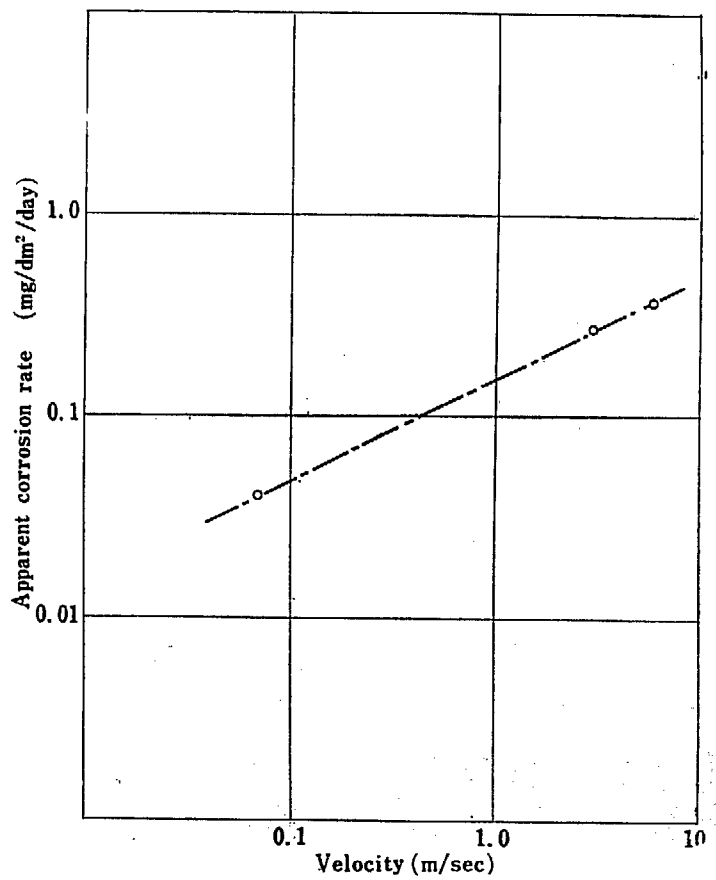

Fig. 11 Apparent corrosion rate vs. flow rate curve at 70°C.

It is shown in TABLE 1 that the values of aluminum increase with the velocity of water and the total amounts of corrosion are influenced by film growth at low flow rate, while they are influenced by dissolution at high flow rates.

The apparent corrosion rates are plotted against the flow rate in Fig. 11, and the following relationship was obtained.

$$|R| \propto \sqrt{V},$$

where R represents the apparent corrosion rate and V represents the flow rate.

The surfaces of the specimens were examined microscopically at each period and some of them are shown in Fig. 12, which show the formation on the surface in the initial stage of corrosion. The size and number of pit were not much affected by flow rate and exposure time, although in some cases of high flow rates the pits extended gradually in the direction of water flow, becoming a long groove.

After exposure in the loop, the surface film was removed from the specimen by the iodine-metanol method and sent to X-ray diffractometry. Because there

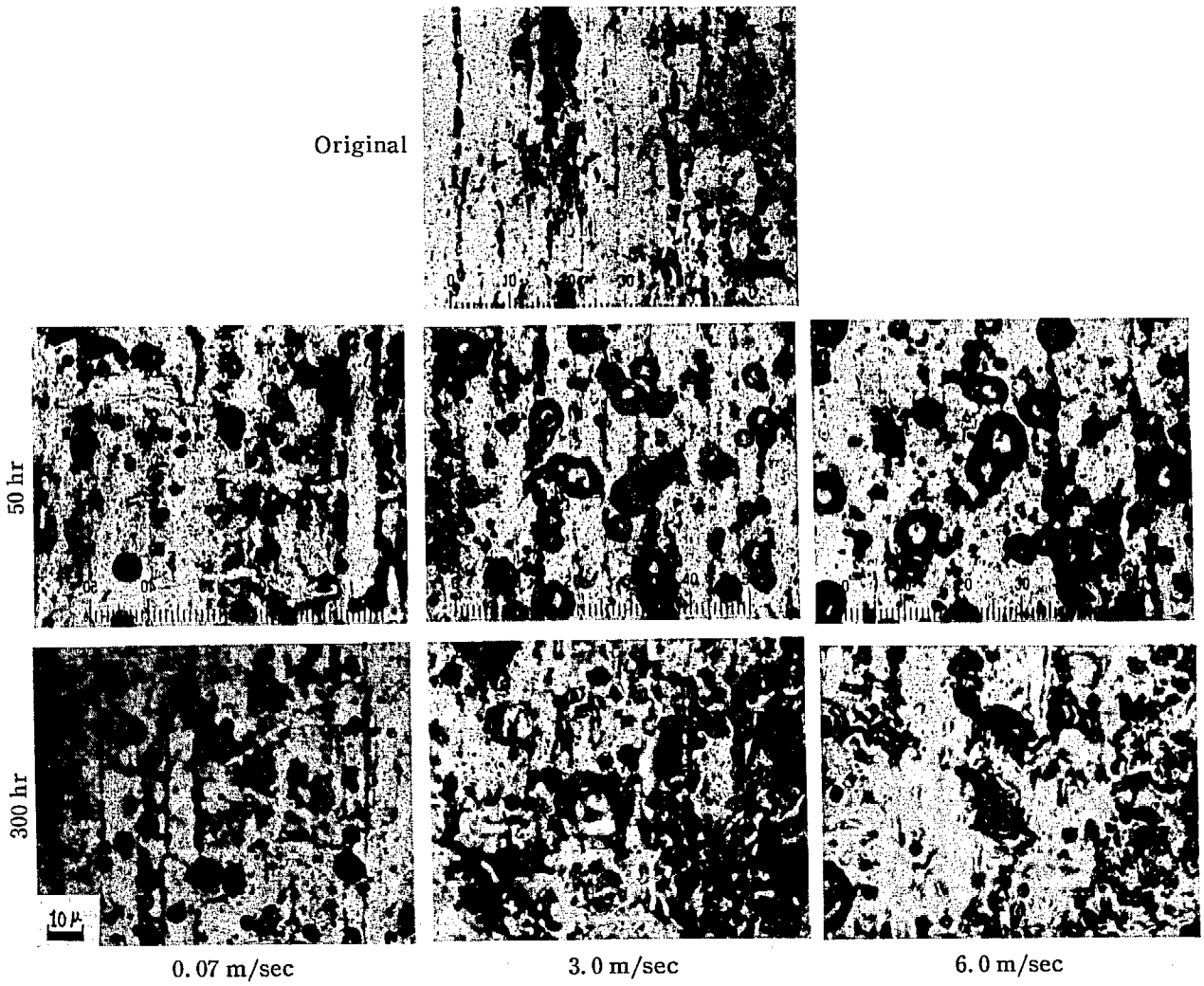

Fig. 12 Surface of specimens corroded in flowing water at 70°C

was no distinct peak in the chart of diffractograph, the surface film was assumed to be amorphous oxide.

B. Programme II The weight change obtained is shown graphically in Fig. 13, and the amounts of metal corroded, dissolved into water and remaining in the surface film are summarized in TABLE 2.

It is seen from TABLE 2 that the corrosion rates in refreshed water are not so much changed by the introduction of gas as those which predicted from the weight change data shown in Fig. 13, and the total amount of corrosion is much influenced by the dissolution of aluminum from specimens, especially when H_2 gas is introduced. It is also found that the dissolution of aluminum is considerable even in non-refreshed water when H_2 or O_2 gas is introduced.

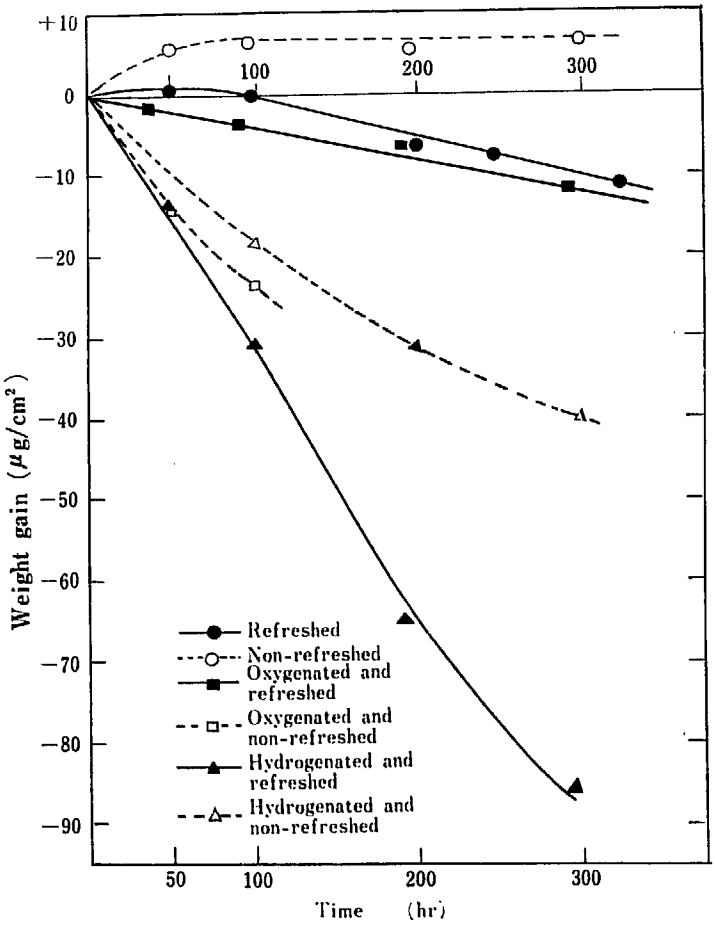

Fig. 13 Weight change of 1100 Al in flowing water at 70°C, 3 m/sec

The thickness of the barrier film produced on the corroded specimens was measured by the HUNTER's method[9]. The voltage-current curves are shown in Fig. 14 from which the specimens were classified into two groups with either thick or thin barrier film. It is interesting that the specimen with a thick barrier film shows a low value of B/A (<2.6) in TABLE 2 while the specimen with a thin film

TABLE 2 Results of corrosion of 1100 Al in flowing water at 70°C, 3 m/sec

Exp. No.	Water condition	Gas supplied	Time period (hr)	A Al in film (mg/dm^2)	B Dissolved Al (mg/dm^2)	B/A ratio	Total amount of corrosion (mg/dm^2)	Corrosion rate ($mg/dm^2/hr$)	Dissolution rate ($mg/dm^2/hr$)	Thickness of barrier film (Å)
1	refreshed	non	320.5	35.6	80.6	2.3	116.1	0.36	0.25	34.4
2		H_2	290	13.0	104.0	8.0	116.9	0.41	0.36	9.5
3		O_2	290	22.8	58.9	2.6	81.7	0.28	0.20	38.7
4	unrefrshed	non	295	6.5	8.6	1.3	15.1	0.051	0.03	43.0
5		H_2	300	10.3	61.7	6.0	72.0	0.24	0.21	13.0*
6		O_2	100	1.6	24.7	15.6	26.3	0.26	0.25	6.5*

* The value is uncertain

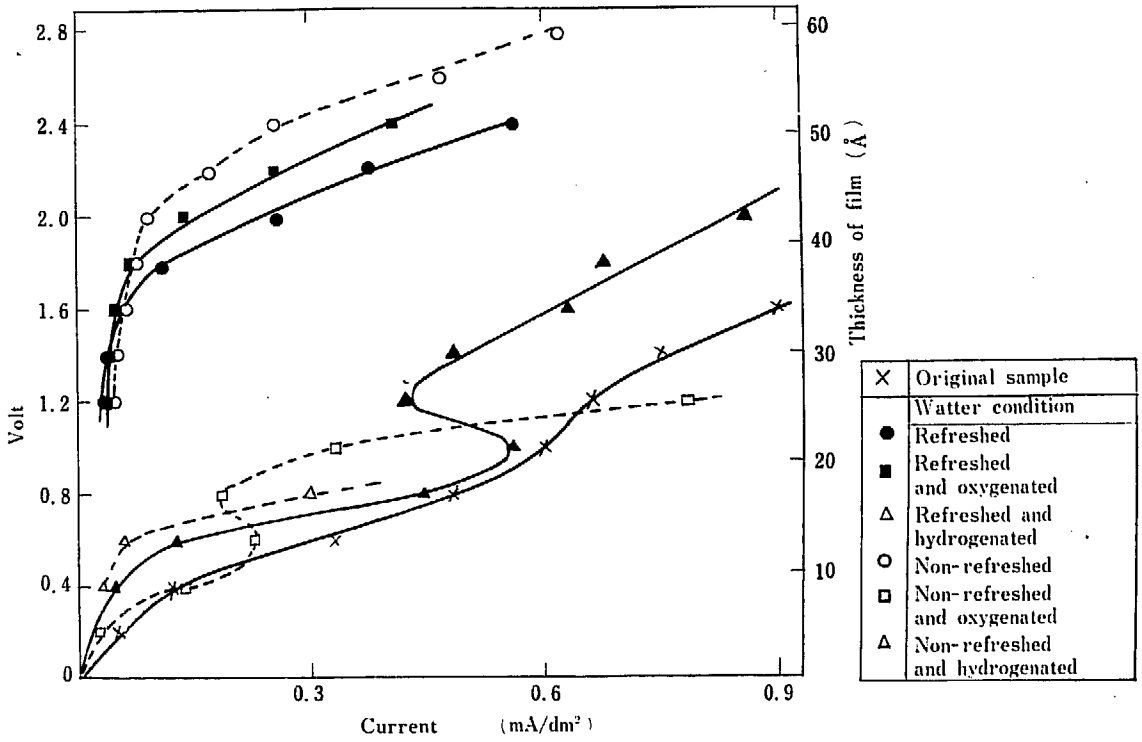

Fig. 14 Current-voltage curves for barrier film thickness measurement

shows a high value (>6.0). Therefore the dissolving tendency of aluminum from specimens into the water seems to be closely related with the thickness of barrier film produced on the surface of specimens.

A new type of dissolution process not attributable to the purity of water must be considered to explain the abnormal dissolution of aluminum in non-refreshed water under H_2 or O_2 atmosphere. In general, dissolution of metal or metal compound (in this case oxide or hydrated oxide) is caused by the following two factors:

(1) dissolution by "solubility"; it depends on the purity of water

(2) electrochemical dissolution by dissolved O_2 and /or impurity ions in water, for instance, Cu, Fe ions, etc.; it depends on the concentration of dissolved O_2 or impurity ions.

It is suggested that the factor (1) is much more operative than (2) in refreshed water whereas the situation is reverse in non-refreshed water. However, even in the case of (2), this process is to be affected by the solubility of corrosion product and it actually ceases when the water is saturated with the corrosion product. Therefore, removal of corrosion product from the specimen must be held to continue the dissolution of corrosion product even in non-refreshed water.

As proposed by HATCHER[9], the mass-transfer process of corrosion products from the specimens to other places in the loop can be applied in this case, instead of the purification process by an exchange column. This process is due to the difference of solubility of corrosion product between two places with different

temperatures in the loop.

Assuming that the contribution of the factor (1) to the total dissolution can be represented by the difference of dissolution rate in non-refreshed water from that in refreshed water, 0.25−0.03=0.22 and 0.36−0.21=0.15 are obtained from TABLE 2 under the conditions of non-gas and H_2- supplied, respectively. Small difference between these values may be explained if the effect of thickness of barrier film on dissolution rate is considered. Under oxygen atmosphere 0.20−0.25=−0.05 is obtained. Although it can not be explained by the above assumption, the following phenomena must be taken into account: in non-refreshed water a large quantity of copper oxide from the valves was deposited on the specimen holder at the points where the specimen was in contact with.

Because copper dissolves easily into the flowing water in the presence of oxygen, the electrochemical dissolution due to the galvanic action between copper and aluminum will strongly occur in non-refreshed water, and the cathodic current seems to exceed the current required for the formation of passive film of aluminum oxide.

The large difference in barrier voltage between the specimens exposed in refreshed water and ion-refreshed water under O_2 atmosphere will provide oue proof for the stable passive film formation.

C. Programme III The results of immersion tests with chemically polished specimens in flowing water at 50°C and 70°C are graphically shown in Fig. 15. The amount of metal corroded increases with time rapidly up to 100 hours, then

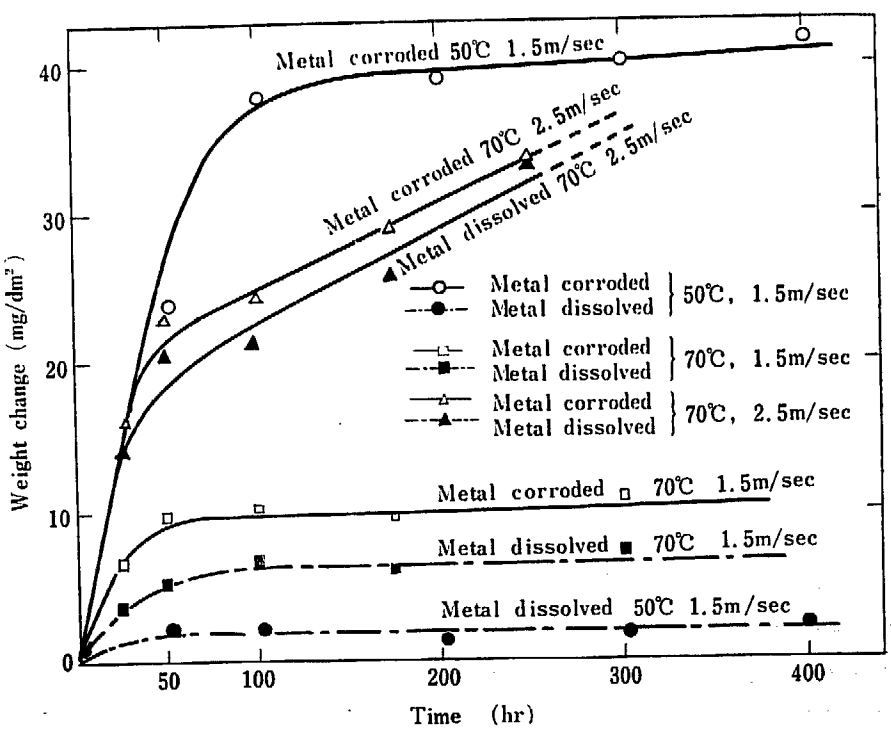

Fig. 15 Weight change of 1100 Al in flowing water

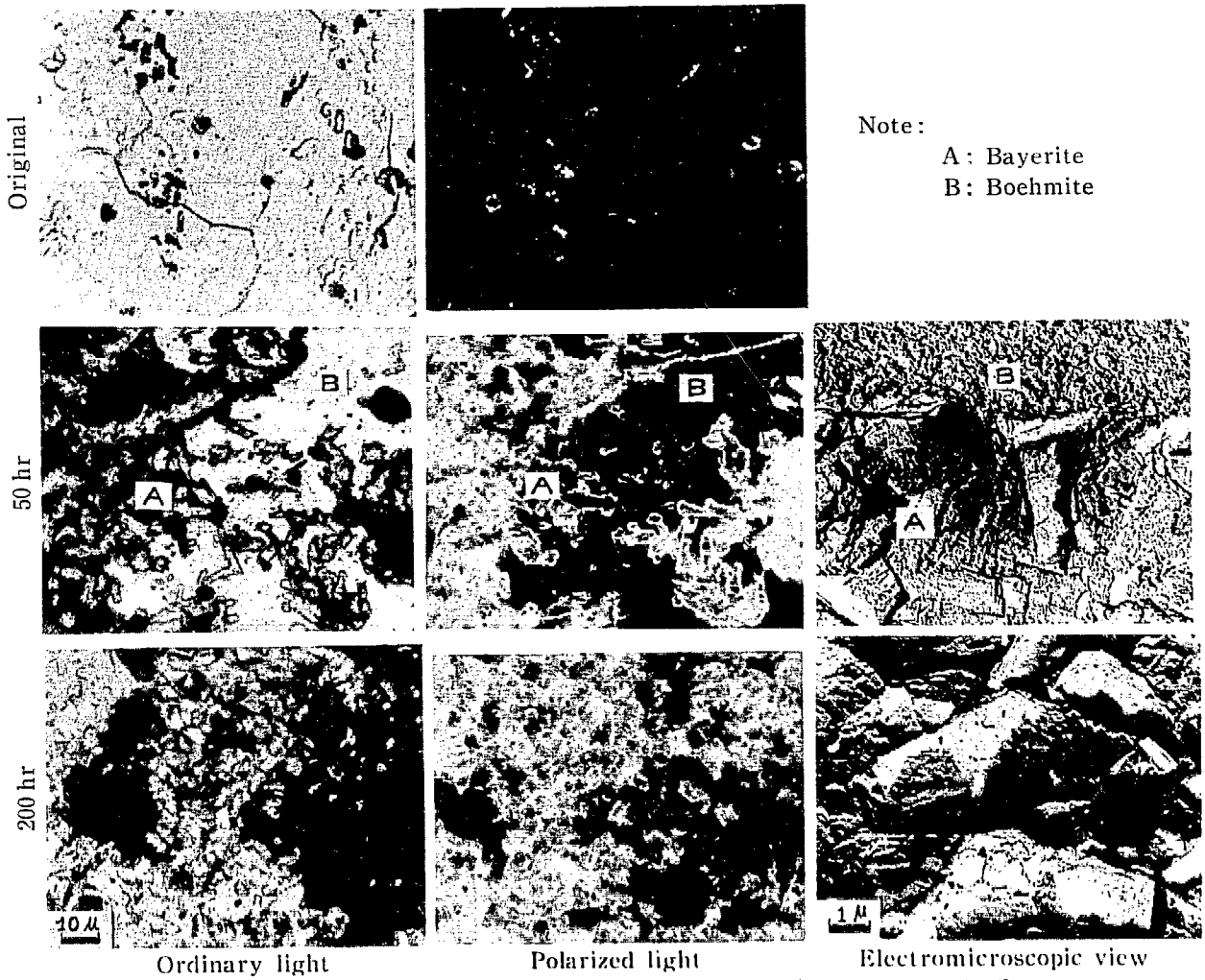

Fig. 16 Surface of specimens corroded in flowing water at 50°C

moderately at 2.5 m/sec of flow rate but very slowly at 1.5 m/sec of flow rate. The ratio of the metal dissolved to that corroded increases with flow rate and especially with temperature.

In the immersion at 50°C the surface structures of the specimens were examined by optical and electron-microscope at each step which are shown in Fig. 16. Bayerite crystals, identified by the X-ray diffraction method, grew on the boehmite film identified by electron diffraction, up to 100 hours corresponding to the rapid increase of metal corroded, and the corrosion reaction actually ceased by the complete coverage of surface with bayerite crystals (Fig. 16). This process may be explained by the dissolution-precipitation process due to the difference of solubilities between boehmite and bayerite. However, at 70°C a few small bayerite crystals with no growth were found on the surface of the specimen and the underlying boehmite layer was observed even after corrosion reaction ceased or slowed down (Fig. 17a). The dissolution-precipitation process does not apply to the above phenomena at 1.5 m/sec of flow rate.

Weight changes of the prefilmed specimens are shown in Fig. 18, in which the

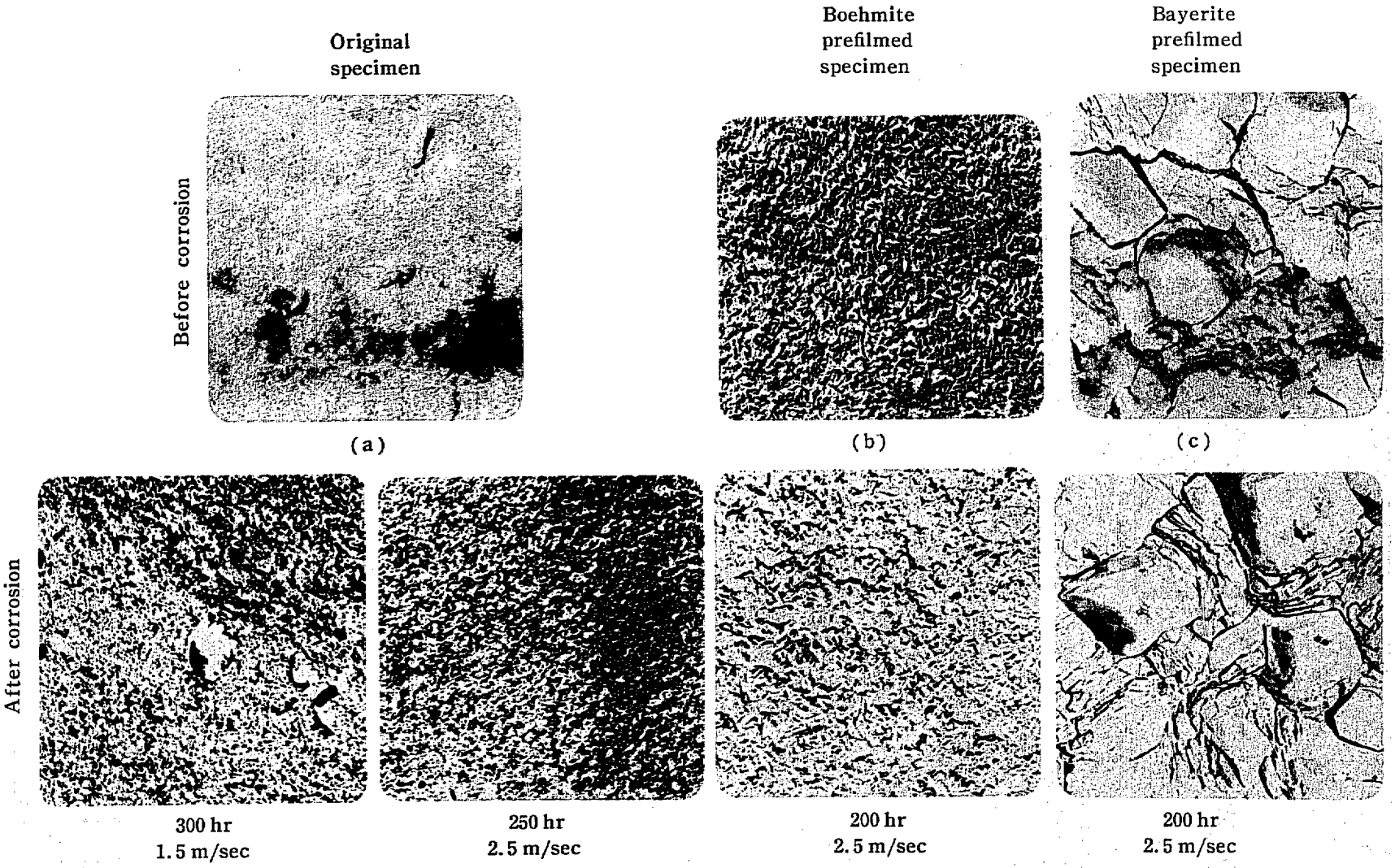

Fig. 17 Electron micrographs of specimens' surface corroded in flowing water at 70°C

bayerite-prefilmed specimens show the increase in weight and the boehmite-prefilmed specimens the decrease in weight with time. It was proved by the comparison of the amounts of metal part before and after the test that the bayerite-prefilmed specimens themselves were not corroded during the test, although the weight increased with time. It is thought, therefore, that bayerite crystals on the bayerite-prefilmed specimens will grow by precipitation of aluminum oxide from the other types of specimens existing in the water. This process will also be explained by the dissolution-precipitation mechanism.

The surface structures of the prefilmed specimens were almost unchanged during the test as shown in Fig. 17.

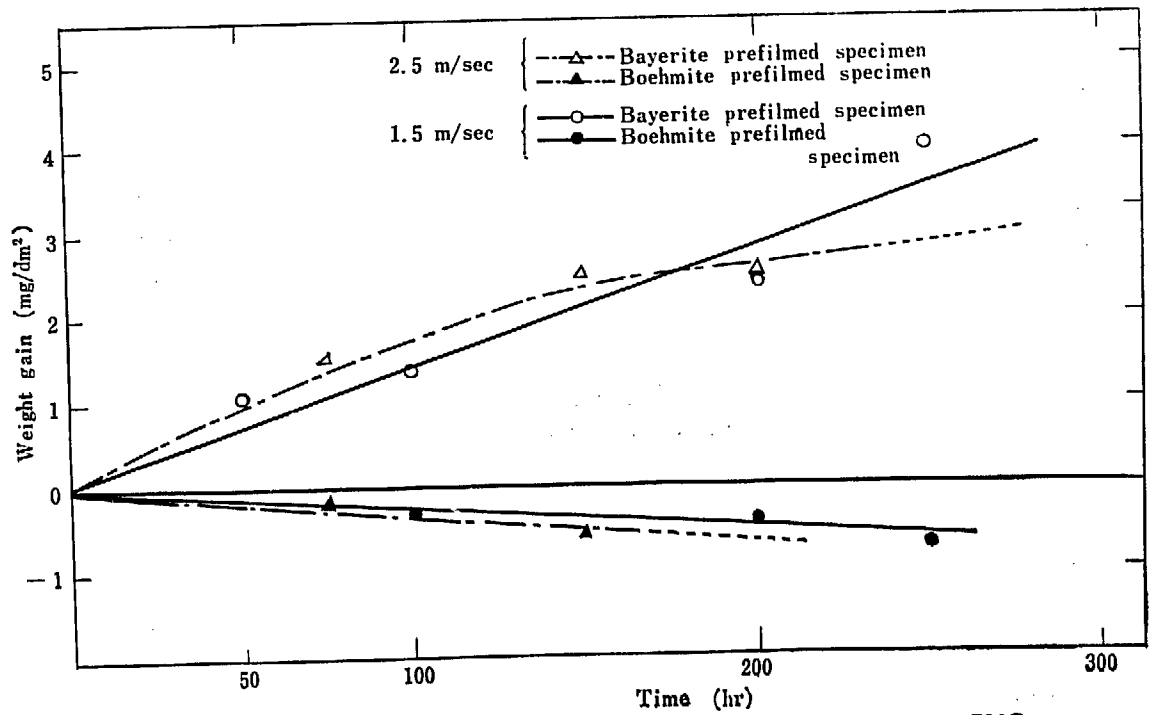

Fig. 18 Weight gain of prefilmed specimens in flowing water at 70°C

A number of pits was observed on all of specimens corroded in flowing water at 50°C and 70°C, but at 50°C pits were covered with corrosion product after 100 hours of immersion.

1.3 Conclusions

The corrosion of 99.99% alminum in stagnant water below 80°C proceeded in the following steps:

1) The first stage; the growth of thin boehmite film proceeds with a logarithmic rate law in the short period after the immersion.

2) The second stage; the corrosion process is governed by the three dimensional growth of bayerite crystals on the underlying boehmite layer based on the dissolution-precipitation mechanism. The nucleation of bayerite has an incubation

time dependent on temperature, but the rate of crystal growth seems to be indedependent of temperature. The activation energy for this stage is calculated to be 4.1 kcal/mole.

3) The third stage; this stage takes place just after the whole surface of the specimen is covered with bayerite, and the logarithmic corrosion rate is decreased. The activation energy for this stage is calculated to be 8.2 kcal/mole.

This stage is indistinguishable from the forth stage at 80°C.

4) The fourth stage; an appreciable increase of corrosion is observed in this stage but the data obtained are too few to be discussed in detail in the present paper.

Some correlations between intergranular attack and boehmite formation are observed.

Dynamic corrosion tests of 1100 aluminum were performed in the following three programmes;

1) Programme I; the corrosion of aluminum in flowing water at 70°C is much influenced by the film growth on the surface of specimen at 0.07 m/sec, and by dissolution of aluminum into the loop water at 3.0 and 6.0 m/sec. A number of pits were observed on all of the specimens tested.

2) Programme II; most of the corrosion in flowing water at 70°C and 3 m/sec is controlled by dissolution of aluminum into the loop water, which is influenced by the purity of water and the thickness of barrier film produced on the surface of corrodied specimens.

The mass-transfer process is proposed to explain the dissolution of aluminum in non-refreshed water. The electrochemical process is also proposed to explain the anomalous dissoltion of alumium in non-refreshed water under oxygen atmosphere.

3) Programme III; the dissolution-precipitation mechanism is successfully applied to corrosion at 50°C and 1.5 m/sec from the observation of the surface structure of specimens and the kinetic study. This mechanism can not be applied to the case at 70°C, but can be applied in the case of prefilmed specimens.

2 CORROSION ABOVE 100°C

2.1 Corrosion in Water

2.1.1 Experimental

Procedure: The static test was conducted using a 5 liter autoclave in which each specimen was placed in a quartz capsule with 150 ml of deionized water (the specific resistance more than 5 MΩ-cm). Prior to the test the system was eva-

cuated by pumping for 5 minutes and then pure argon was introduced. At the each removal of specimens for the examination both the specimens and water were replaced by the new ones.

Specimens: The specimens used were three kinds of pure aluminum and several 99.99%-base aluminum alloys as shown in TABLE 3 and 4.

TABLE 3 Composition of pure Al samples

Nominal purity	Al	Si	Fe	Cu	Mn	Mg	Zn
99 % Al	99.150	0.18	0.64	0.02	0.01	tr	tr
99.9 % Al	99.937	0.024	0.036	0.003	tr	tr	tr
99.99% Al	99.992	0.005	0.001	0.002	tr	tr	tr

TABLE 4 Chemical composition of Al alloy samples

Component / Nominal composition	Fe (%)	Si (%)	Cu (%)	Ni (%)	Zn (%)	Mn (%)	Mg (%)
Fe 0.5%	0.52	0.05	0.01	—	—	—	—
Fe 1 %	1.04	0.02	0.01	—	—	—	—
Fe 2 %	1.92	0.05	0.01	—	tr	0.01	—
Si 0.5%	tr	0.49	0.01	—	—	—	—
Si 1 %	tr	0.83	0.01	—	—	—	—
Si 2 %	0.02	2.10	0.01	—	tr	tr	—
Ni 0.5%	tr	0.02	0.01	0.53	—	—	—
Ni 1 %	0.04	0.04	0.01	0.94	—	—	—
Ni 2 %	0.05	0.04	0.01	1.99	tr	tr	—
Cu 1 %	tr	0.01	0.98	—	—	—	—
Cu 2 %	tr	0.03	1.85	—	—	—	—
Zn 1 %	tr	0.02	0.01	—	1.13	—	—
Mg 1 %	tr	0.02	tr	—	—	—	0.99
Mn 1 %	0.01	0.02	0.01	—	—	1.03	—

They were tested mainly in the shape of rolled rectangular coupons (50×20×1 mm) except in some alloys which were also tested in the shape of tablet machined from the ingots for metallographic study. The specimens were pretreated by the same method as described in 1.1.1.

Examination: The corrosion amount was determined mainly by the apparent weight gain, and if necessary, by the chemical analysis of dissolved aluminum[10] and/or by the weighing of the corrosion product using the iodine-methanol method[11]. The results were evaluated at least by the average of four specimens.

In the post-exposure examination, emphasis was placed on the microscopic examination of the surface and cross section of the sample, and the X-ray diffraction method was applied to the determination of the oxide removed from the specimen.

2.1.2 Summary of the Results and Discussion

a) The factors affecting the intergranular attack on pure aluminum[12]

Impurities in metals: Three kinds of aluminum (TABLE 3) were tested at the various temperatures up to 250°C. It was confirmed that the extent of intergranular penetration and the total amount of corrosion increased with increasing the purity of metal but only 99% aluminum was corroded uniformly, forming a protective film. One of the results is illustrated in Fig. 19.

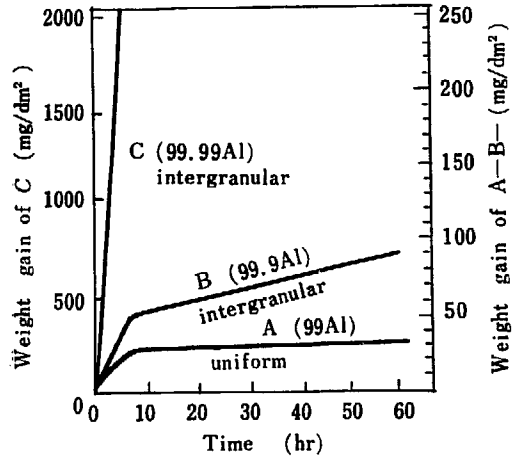

Fig. 19 Corrosion of Al in deionized water at 200°C

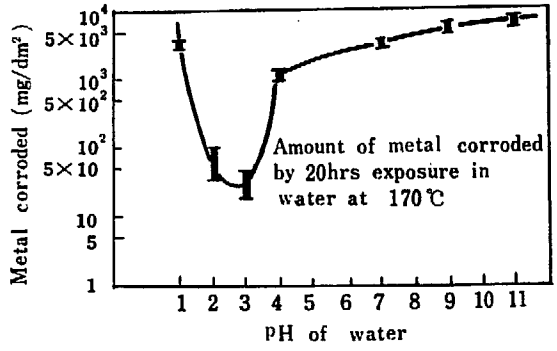

Fig. 20 The effect of pH of water on the corrosion of pure Al

Effect of the crystal grain size: The intergranular corrosion of 99.99% aluminum, of which the grain size was controlled by the strain-annealing method, was examined microscopically.

The depth of intergranular penetration at each boundary was independent of the grain size, so that the total amount of corrosion was approximately proportional to the boundary density. Thus it was suggested that there should not be expected a role played by the electrochemical polarization at the boundary.

Effect of pH of water: Several tests were performed in water of different pH prepared by addition of KOH or H_2SO_4. The intergranular attack was markedly affected by pH. The total amounts of corrosion are shown in Fig. 20. The total corrosion was minimized at pH 3 where the intergranular susceptibility to the attack of 99.99% aluminum was eliminated, and the weight changes turned negative below pH 3.

Both uniform and intergranular corrosions seem to have a close relation with the concentration of H^+ ion even if the effect of $SO_4^=$ or K^+ ion is ignored.

Effect of cold working: A remarkable change was observed in the corrosion behavior of cold worked 99.99% aluminum specimens as seen in Fig. 21 and TABLE 5.

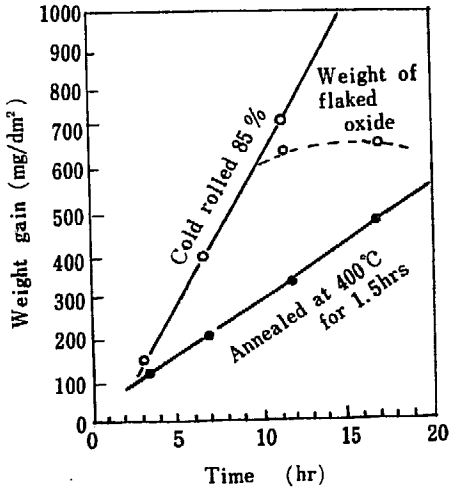

Fig. 21 Effect of cold rolliong on corrosion rate of 99.99% Al in deionized water at 150°C

TABLE 5 Corrosion of cold rolled 99.99% Al in deionized water at 170°C

Reduction by rolling (%)	0	10	35	85
Weight gain	969	1241	1156	810
Removed corrosion product	0	15	165	288
Total weight increase (mg/dm²)	969	1256	1321	1098

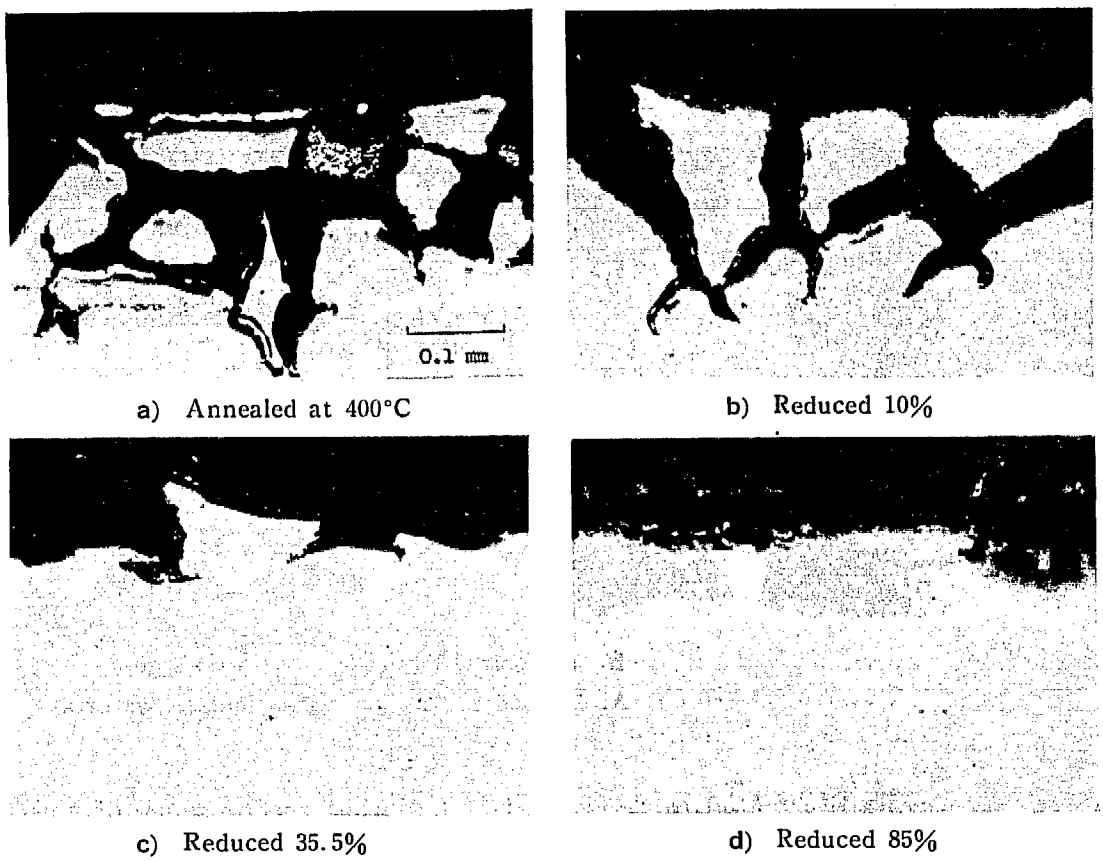

a) Annealed at 400°C b) Reduced 10%

c) Reduced 35.5% d) Reduced 85%

Fig. 22 The effect of cold rolling on the intergranular attack of 99.99% Al exposed for 20 hours in deionized water at 170°C (cross-sections) (×100)

The intergranular penetration was reduced with the increasing degree of cold rolling as shown in Fig. 22; however the spalling and crystallization of the surface film increased as understood from the results in Fig. 21 and TABLE 5. It was also

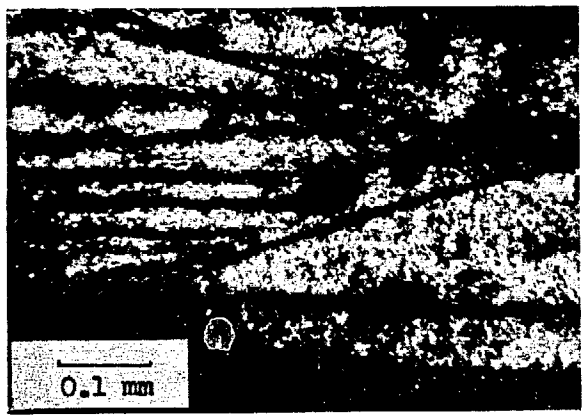

Fig. 23 Microsurface of 99.99% Al exposed for 2 hours in deionized water at 170°C under hydrogen atmosphere. Localized attacks are observed on slip clusters formed by cold rolling. (×100)

noted that the slip clusters formed by the cold work were preferentially attacked in a similar manner to that for the attack at grain boundaries as seen in Fig. 23.

Effect of atmospheric gases: In order to examine the effect of hydrogen on the intergranular attack of 99.99% aluminum, hydrogen or oxygen was introduced into the system instead of argon.

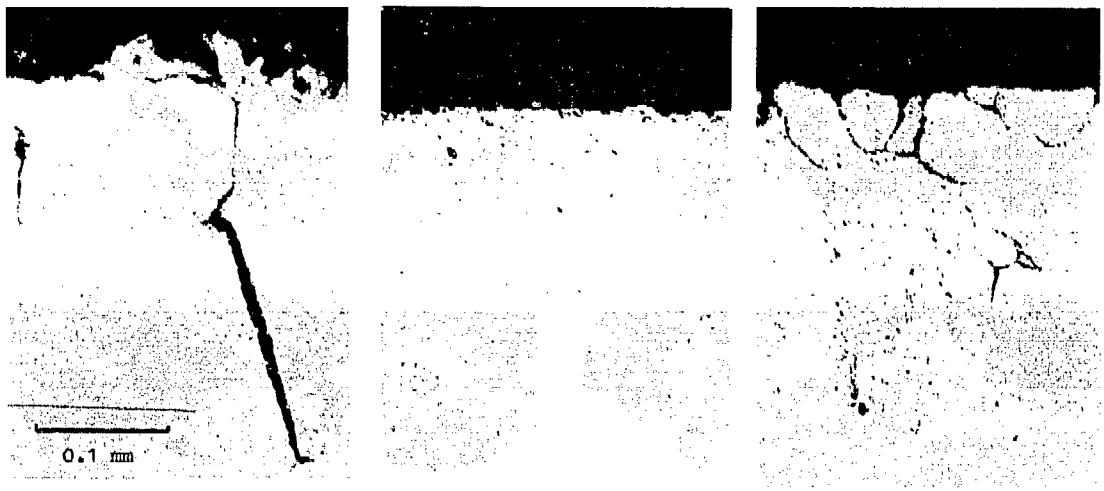

a) Hydrogen b) Oxygen c) Argon

Fig. 24 Cross sections of 99.99% Al exposed for 20 hours in deionized water at 170°C under various atmospheres (×150)

From the results illustrated in Fig. 24 it is found that the presence of a certain amount of hydrogen obviously accelerates the penetration, while oxygen entirely eliminates it at 200°C although the total corrosion is increased. Moreover, it is noteworthy that there was a close relation between "atmospheric" hydrogen and defect sites formed by rolling as seen in TABLE 6; the effect of cold work was made larger in the presence of hydrogen while a quite opposite effect was observed with oxygen.

TABLE 6 Weight gain of cold worked Al by corrosion in 150°C water under various atmospheres

Enclosed gases	Pressure at room temperature (atm)	Reduction by cold rolling		
		0%	35.5%	85%
A	5	76	75	156
A	15	121	96	153
H_2	5	150	150	217
H_2	15	119	119	196
O_2	5	26	24	25
O_2	15	140	121	121

(mg/dm²)

Summarizing the above results it is evident that the factors examined have, more or less, the relation with the corrosion product hydrogen, which is supposed to be atomic and to play a destructive role through grain boundary diffusion.[13),14)] However, it should be noted that there is another important factor which will be discussed in 2.2, i.e., hydration of oxide.

b) Effect of alloying elements on the corrosion of pure alminum[15)]

Corrosion of rolled sheet: Each of the elements Fe, Ni, Cu, Si, Mg, Mn and Zn were added 0.5 to 2% into 99.99% aluminum; the results obtained with these alloys, at 300°C are shown in TABLE 7. The susceptibility to the intergranular corrosion was observed in the alloys of 0.5% addition but not in the alloys of more than 0.5% addition of Fe, Ni, Cu and Si, as shown in TABLE 8. The alloys with

TABLE 7 Corrosion of Al alloys in deionized water at 300°C (weight gain in mg/dm²)

Sample \ Time	5 min	30 min	3 hr	20 hr	48 hr	95 hr	290 hr
Fe 0.5	67	496	2141	5907	*	failed	—
Fe 1	30	30	29	29	30	228	1500
Fe 2	25	32	33	51	198	645	—
Si 0.5	7200	*	failed	—	—	—	—
Si 1	4500	6300	failed	—	—	—	—
Si 2	734	2100	3142	failed	—	—	—
Ni 0.5	251	435	736	993	*	failed	—
Ni 1	34	32	41	43	49	60	90
Ni 2	30	32	31	32	37	46	60
Cu 1	91	250	1470	failed	—	—	—
Cu 2	29	30	32	89	412	*	—
Zn 1	failed	—	—	—	—	—	—
Mg 1	failed	—	—	—	—	—	—
Mn 1	failed	—	—	—	—	—	—

* immeasurable

TABLE 8 The effect of alloying addition on the type of corrosion of Al exposed for 20 hours in deionized water at 200°C

Alloying element \ %	0.5	1	2
Fe	I	H	H
Ni	I	H	H
Si	I	I	H
Cu	—	I + P	H

I : Intergranular corrosion
H : Homogeneous corrosion
P : Fine pitting corrosion

Zn and Mg showed a deep intergranular penetration and the alloy with Mn was non-resistant due to the spalling of oxide. All of alloys except Ni showed a corrosion-rate transition after a short exposure. However, it was noted that the weight gain in the uniform corrosion stage was about 30 mg/dm² among all the alloys. The results obtained are shown in Fig. 25 and 26. The X-ray diffraction of the surface oxide showed that the nearly amorphous film produced in the early stage turned into well crystallized boehmite at the rate-transition point.

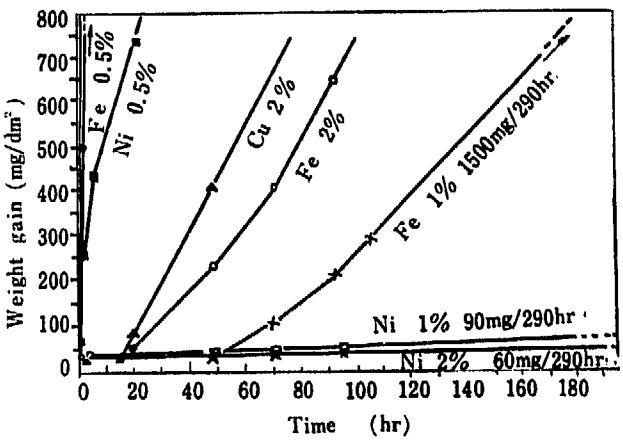

Fig. 25 Corrosion of Al alloys in deionized water at 300°C

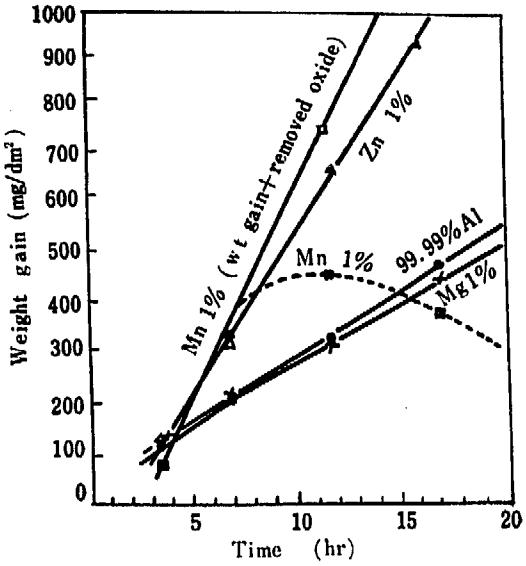

Fig. 26 Corrosion of Al and Al alloys in deionized water at 150°C

The local penetration in alloys: In the early stage of corrosion the second phases in Al-Ni and Al-Fe alloys, thought to be cathodic against the primary phases, seemed to be corroded locally, but in the Al-Fe alloys it was observed that the primary phase was preferentially attacked after the break-away, shown in Fig. 27 a) and b).

It seems that the effect of "alloying" is of considerable significance in the corrosion of aluminum, and that a certain amount of Ni, Fe, etc. alters the proper-

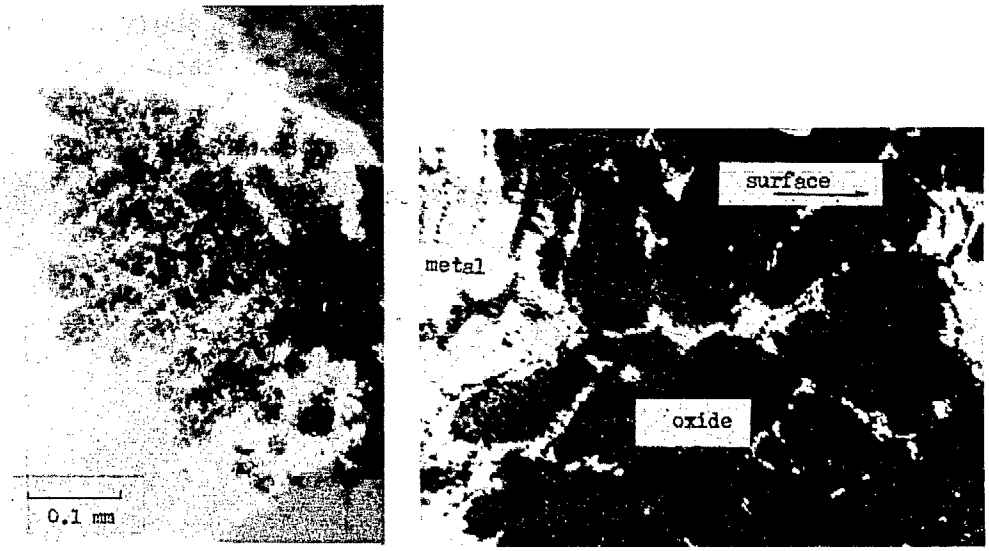

a) Al-0.5% Fe alloy b) Al-2.0% Fe alloy

Fig. 27 Cross section of heavily corroded Al-Fe alloy ingots exposed for 48 hours in deionized water at 300°C

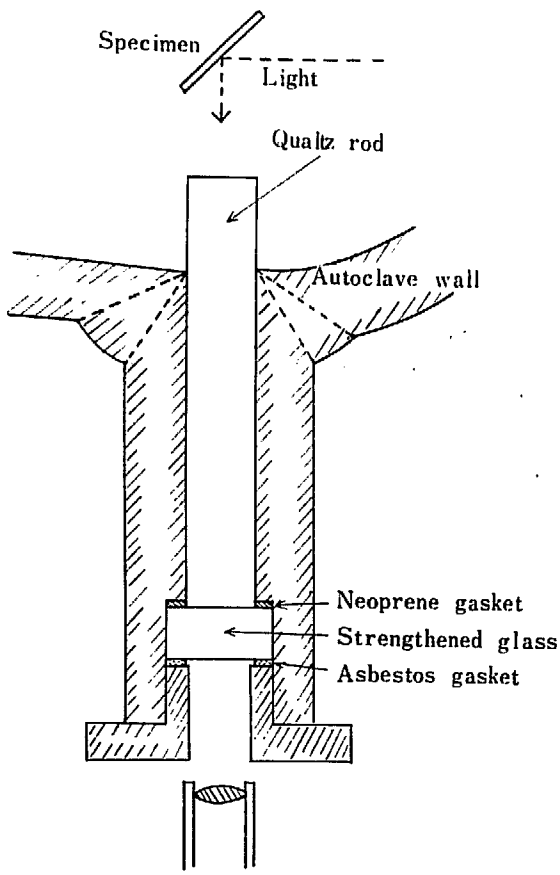

Fig. 28 Schematic drawing of window for direct microscopy

ty of grain boundary. The preferential penetration of the primary phase may be due to the preferential hydration and crystallization of the surface oxide, as will be described in 2.2.

c) Direct observation of high temperature corrosion

The viewing autoclave with the windows specially-designed to avoid the effect

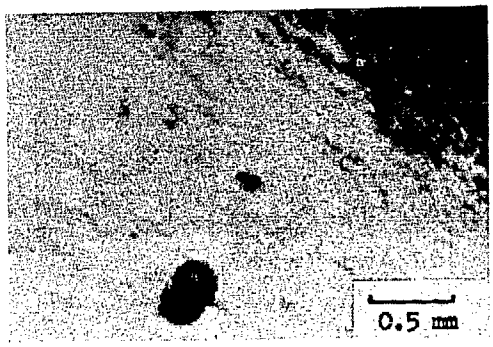

a) 50 min
Hydrogen bubbles are formed at a few points.

b) 180 min
Homogeneous interference-red colour was appeared.

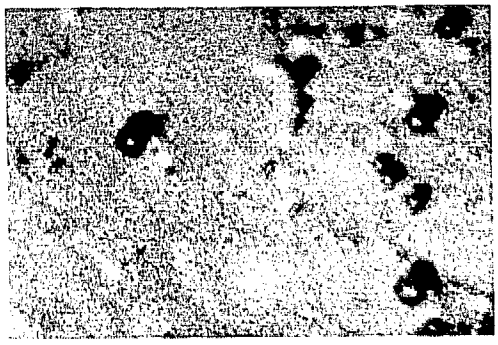

c) 200 min
Suddenly bright surface turned to the dull and the grain boundry became visible accompanied with increased bubble formation.

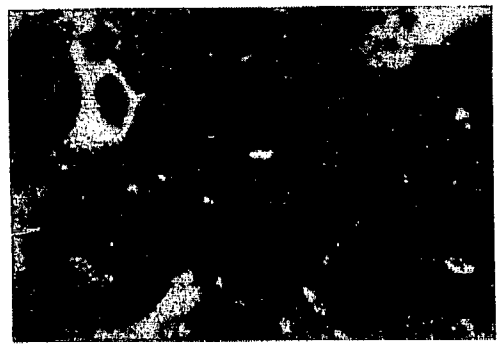

d) 17.5 hr
Partial intergranular attack takes place in 5 hr and proceed on with a lot of hydrogen formation from the gap.

e) 24 hr
Almost all the boundaries are attacked.

Fig. 29 Direct observation of intergranular attack (99.99% Al)

of thermal convection was employed (Fig. 28).

The series of micrographs in Fig. 29 show the kinetic process of intergranular attack on 99.99% aluminum, in which hydrogen generation was observed at the boundary portion. Figure 30, the cross section, indicates the formation of hydrogen

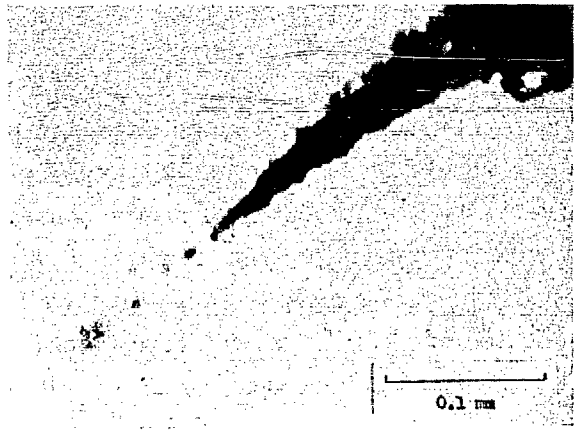

Fig. 30 Hydrogen bubble leading intergranular attack
(99.99% Al, 200°C, 24 hr)

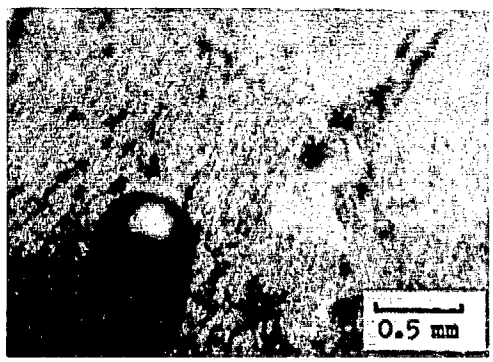

a) 165°C 35 min
A bubble is formed on a point.

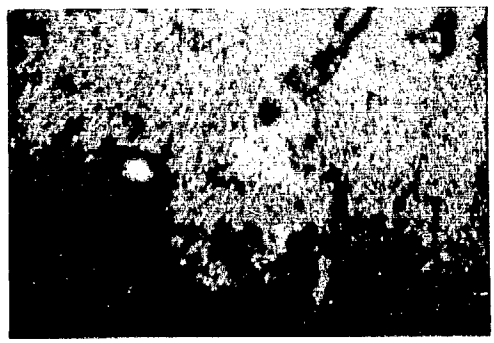

b) 60 min

c) 75 min
The bubbling increases.

d) 95 min
The system is cooled down to 120°C.
A pit had been formed at the point of bubbling.

Fig. 31 Direct observation of kinetic process of pitting corrosion caused by the presence of copper in water

bubbles at the grain boundary, which is thought to lead the penetration. (The process of pitting corrosion was observed as shown in Fig. 31, when copper existed in the water.)

2.2 Corrosion in Steam[16]

2.2.1 Experimental

Many confusions were caused in the kinetic data and oxide structure because of the use of slowly-heated autoclaves in the earlier experiments.

The improved procedure used in the present study consisted of two autoclaves which were connected with a spiral pipe held at the test temperature as shown in Fig. 32. Then it was possible to supply steam with well-controlled temperature and pressure to the preheated specimens which were placed to accept uniform heat radiation from the wall; the specimen hanger, made of alumina, was designed to divert condensed water drops away from the specimen. The test section was first filled with pure argon by several repetition of evacuation and filling, and when the test section was brought to the test temperature the heated steam was instantaneously introduced to the test section. The desired condition was usually attained 3 minutes or less after the releasing of the valves. At the end of the exposure steam was blown out and then cold argon was introduced during the dismounting of the specimens to prevent the heat effect.

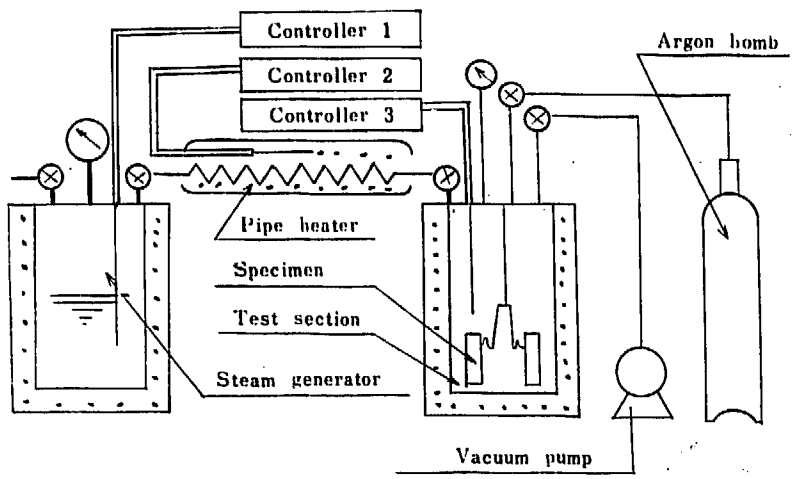

Fig. 32 Schematic drawing of testing procedure

Two kinds of specimens as shown in TABLE 3 were used. The corrosion of both specimens in water was well known by the previous study. They were prepared in the same way as already described in 1.1.1. Sample of oxide powder for hydrothermal treatment was exposed to steam, wrapped in a fine mesh of stainless steel.

The gravimetric method was employed for corrosion measurement and the

result was evaluated by the mean value in the area of at least 240 cm^2 within the accuracy of 1.3 $\mu g/cm^2$. After weighing, the specimens were examined with an electron- and optical microscope followed with the X-ray and electron diffraction. Finally the specimens were examined in regard to hydrogen agglomeration with an optical microscope for which the tapersection method was applied.

2.2.2 Results and discussion

Kinetic observation: The apparent fashion of corrosion in this temperature range closely resembled that of aqueous corrosion, and the results obtained for 99.99% Al specimens were obviously paraboric in time dependence as shown in **Fig. 33.**

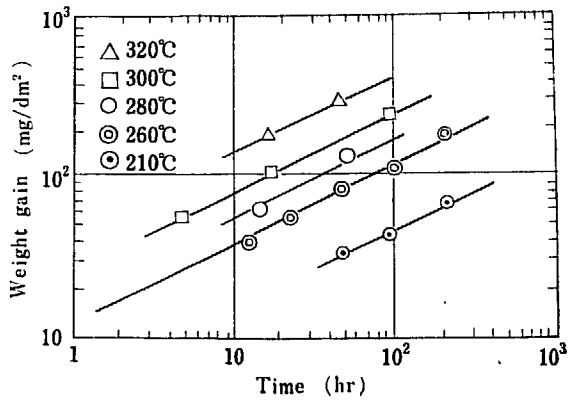

Fig. 33 Corrosion of 99% Al in saturated steam up to 320°C

According to CABRERA-MOTT's theory[4] on the paraboric oxidation rate the result obtained above is thought to correspond to the diffusion-controlled paraboric rate process. Then the paraboric constant was obtained in the equation

$$\Delta W^2 = k_p \cdot t \qquad (5)$$

where ΔW, k_p and t denote the weight change, paraboric constant and exposure time, respectively; the constant k_p has generally the temperature dependence as given by the equation

$$k_p = A \cdot \exp(-\Delta H/RT) \qquad (6)$$

where A is the constant, frequency factor, and ΔH, R, T represent activation energy, gas constant and absolute temperature, respectively.

Figure 34 is a logarithmic plot of k_p against reciprocal temperature from which the activation energy ΔH is calculated to be about 32 kcal/mole using the equation (6). The value 32 kcal/mole is found to be close to those calculated from the result[17] of the break-away-induction time for the corrosion of an aluminum alloy in water and steam in the same temperature range; both are about 31 and 35 kcal/mole, respectively, assuming the corrosion amount in the induction period to be paraboric against time.

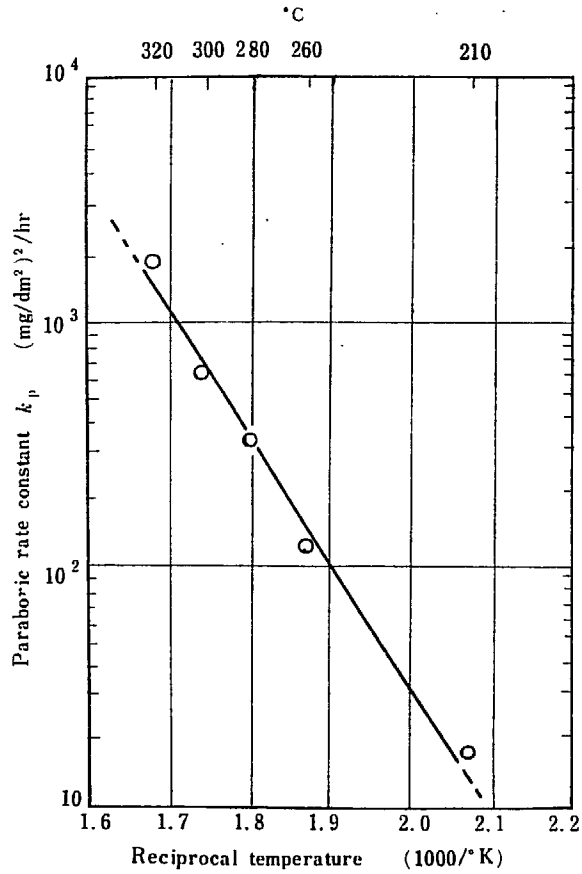

Fig. 34 Effect of temperature on paraboric constants of corrosion

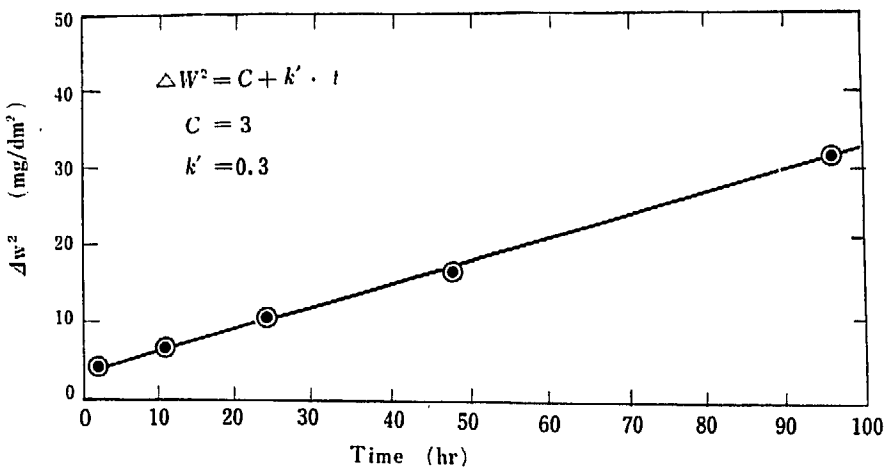

Fig. 35 Corrosion of 99% Al in superheated steam at 260°C, 30 kg/cm²

It was also observed that there was a large pressure dependence of corrosion when the result of Fig. 35 is compared to Fig. 33 which can not be expected from the WAGNER's mechanism[18] for the pressure dependence of oxydation. WILKINDS and WANKLYN observed that there existed the relation between corrosion amount and pressure represented by the formula $\Delta W = k \cdot P^4$ at 325°C[19]. Since it is rather dif-

ficult to understand the corrosion mechanism by the simple diffusion of aluminum ions through the oxide layer, another process controlled by migration of some hydrogen-bearing carries such as OH^- or H_2O may be thought to mainly contribute to the inward-hydration and recrystallization of oxide, which will tend to reduce the protective nature of oxide film. In general the diffusion-controlled oxidation is thought to proceed with increasing thickness of protective film; whereas the present case has the tendency to decrease the barrier thickness, although the distance of the diffusion path is increassed in the outer hydrated portion. This is considered to cause the increase of corrosion amount or of the frequency factor, A, in the equation (6).

As generally known aluminum has a double layered film in the thermally formed oxide[20),17)]. In the present experiment, as will be described later, a distinct double layer was observed (Fig. 36). DILLON and TROUTNER pointed out the outer layer, which is hydrated and crystallized, is porous but occupies almost all the thickness of the oxide, so that it will naturally be thought that the diffusion in the outer layer is more probable to control the corrosion process than that in the inner layer, which is anhydrous and amorphous, although the latter has a higher specific resistance. However the oxidation reaction depends also on the activation process through the barrier layer which, however, is restricted its growth by the inward-hydration process, in other word, the direction of the growth of inner- and outer layer is opposite each other so that the latter process, the destructive, serves as a controlling step.

Oxide film: All the film produced in steam in this temperature range were determined to be boehmite, almost independent of steam dryness. In most cases they had a distinct layer-structure which is typically shown in Fig. 36; the outer white layer was well-crystallized boehmite and the inner grey layer was amorphous, slightly hydrated oxide, supposed to be ρ-alumina from the single dull peak in Fig. 36.

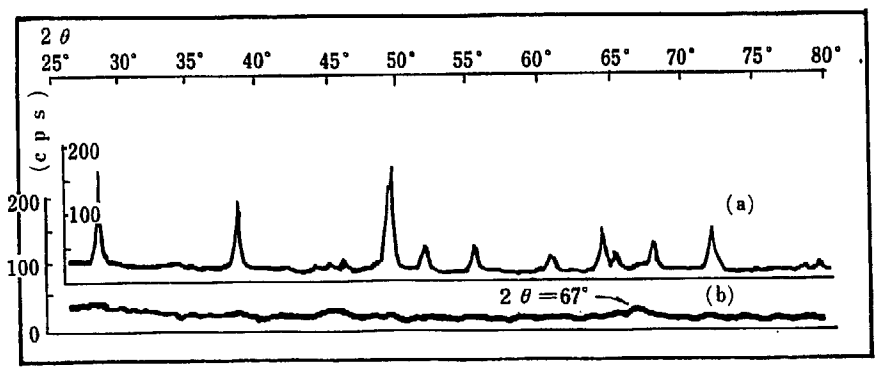

(a) Outer film, boehmite α—ALOOH
(b) Inner film, ρ—alumina ?

Fig. 36 X-ray diffraction of inner and outer oxide formed during the corrosion in saturated steam at 260°C

On the other hand, the electron micrographs as shown in Fig. 37 represent the crystal growth of boehmite in saturated steam, which was considerably rapid in the case of 99.99% Al specimen and destroyed by the intergranular attack rapidly as illustrated in TABLE 9.

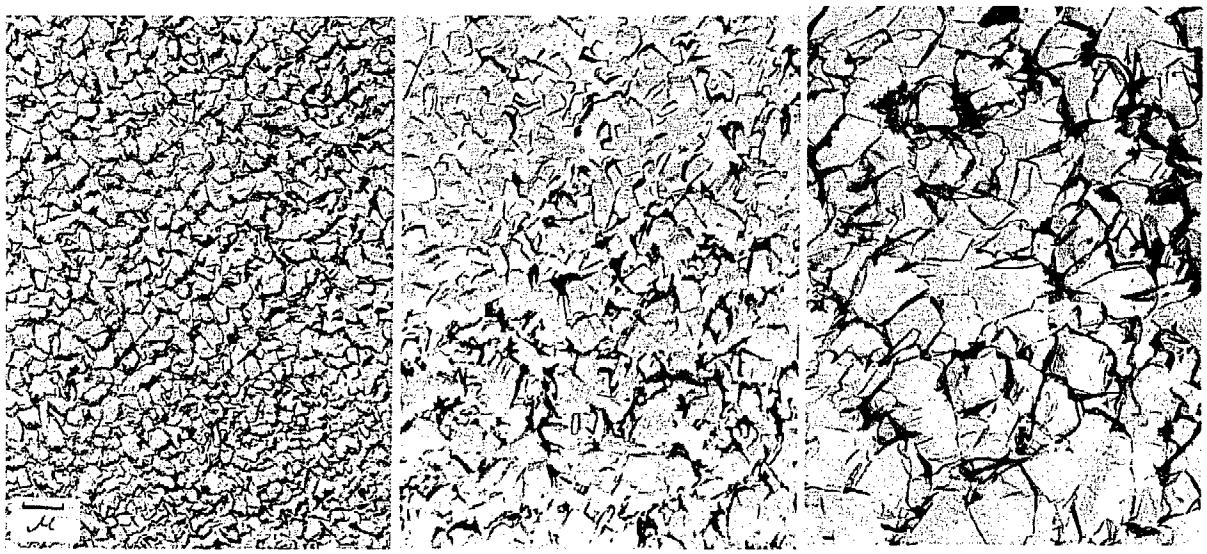

a) 3 hr b) 96 hr c) 212 hr

Fig. 37 Crystal growth of boehmite (α-AlOOH) film formed on 99% Al in saturated steam at 260°C

TABLE 9 Corrosion 99% and 99.99% Al by short time exposure in saturated steam at 260°C

Time / Sample	7 min	20 min	30 min	60 min	
99% Al	5.6	14.0	16.5	—	
99.99% Al	105	445	530	640	weight gain in mg/dm²

b) Corrosion in superheated steam in higher temperature range

Kinetic consideration of the penetration attack: The several experimental series performed in which the steam pressure was varied from 15 to 100 kg/cm² at 350 and 400°C, the following conclusions were obtained.

The weight changes were neglegibly small (1~3 μg/cm²) and penetration-induction time was so short that the corrosion rate was not determined. The penetration attack observed had a peculiar nature just as reported by other workers[21),19)]. It started at random spot and extended in the circular shape as illustrated in Fig. 38. The reason they often start at the edge and extend only parallel to the surface plane of the plate is understood experimentally to the preferential diffusion of hydrogen through the rolling-annealing texture of the specimen. The destructive action of hydrogen will be described later.

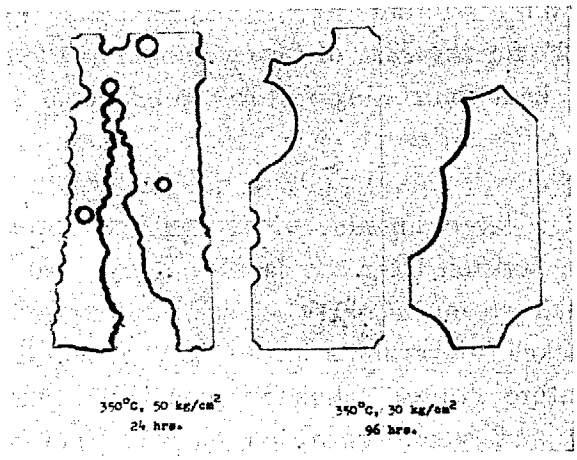

Fig. 38 Macro-view of penetration attack on 99% Al exposed for 48 hours to superheated steam at 350°C

It is noted that the attack-induction time depends largely on the steam pressure rather than on temperature. From the result given in Fig. 39 the relation (7) is derived;

$$t_i = C_1 \cdot P^{-4} \tag{7}$$

where t_i, C_1 and P represent the penetration-induction time, constant and steam pressure, respectively.

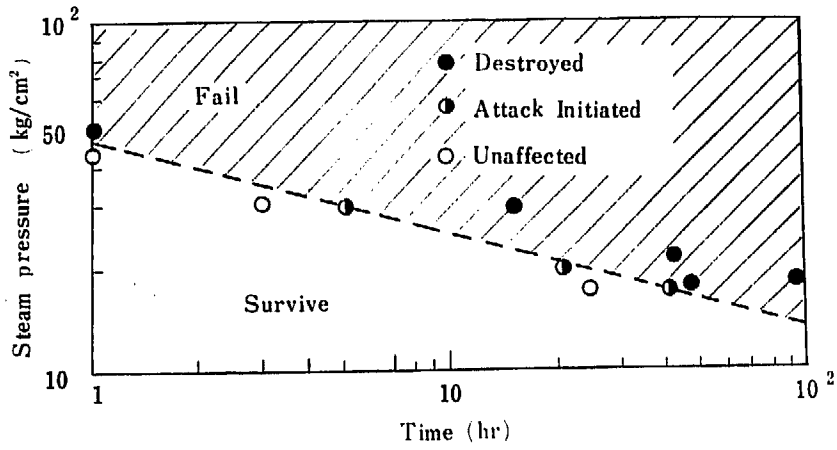

Fig. 39 Effect of steam pressure on penetration-induction time of 99% Al at 400°C

The equation (7) is converted to

$$k = C_2 \cdot P^4 \tag{8}$$

where k is the rate constant in the induction period, when assuming;

i) The penetration attack is initiated by a critical amount of corrosion products such as the surface oxide or hydrogen dissolved in metal.

ii) The corrosion rate law is not altered by the pressure change, just as in the case of lower temperature already shown in Fig. 35.

Above result is quite similar to the experimental equation established by WILKINS and WANKLYN[19] for the case of lower temperature (325°C). This fact suggests that there may be a controlling factor related to the steam condition because the surface oxides are quite different each other. Then the migration process of some hydrogen-bearing carriers might play a role in both higher and lower temperature ranges, because a large amount of hydrogen is absorbed in metal at higher temperatures as will be written later. It is also noted that the 99.99% aluminum survived in superheated steam at 400°C more than twice the time for the 99% specimen and was attacked intergranularly. This is much different from the results for the lower temperature range. Thus it is concluded that the inferiority of pure aluminum in aqueous and steam corrosion as well as the susceptibility to the intergranular attack may be due to the nature of the oxide film which is less resistant against the hydration in boehmite forming range. The preferential hydration at the grain boundary is thought to be due to the local depletion of the surface energy which is supposed to be maintaining the stability of the inner barrier layer, since the grain boundary energy is supposed to be larger in super purity aluminum. Those interpretation will be supported by the result in C).

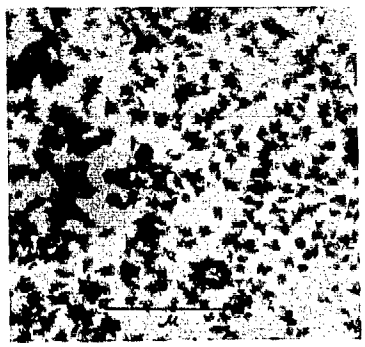

a)
Nuclei of α-Al_2O_3 in amorphous matrix. (99.99% Al in 35 kg/cm²-steam, 3 hr)

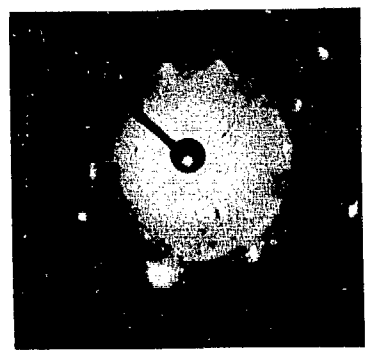

b)
Micro diffraction of (a) shows pattern of α-Al_2O_3

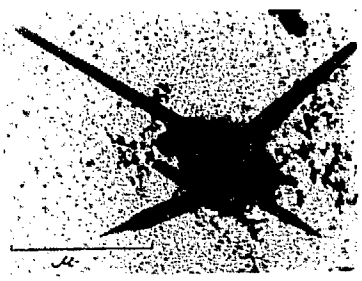

c)
Whisker growth on the surface of oxide film. (99% Al in 18 kg/cm²-steam, 3 hr)

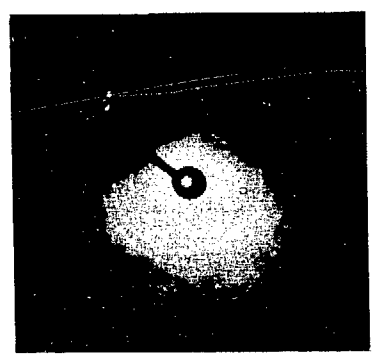

d)
Micro diffraction of (c) shows pattern of α-Al_2O_3 including larger single crystals.

Fig. 40 Transmission electron micrographs and diffraction patterns of surface films formed in steam at 400°C

Corrosion product oxide: The corrosion product formed by the penetration attack were found to be α-Al_2O_3 with one following exception; ρ-alumina was once formed at 350°C which were also observed in the inner layer formed in saturated steam at 300°C. It is noteworthy that little corrosion, with the original brightness remaining and even no interference color appearing, which enabled the transmission electron microscopy of the thin film. Figure 40 a) to d) indicate that the film consists of the fine nuclei of α-Al_2O_3 dispersed in the amorphous matrix and there were observed the whiskers of α-Al_2O_3 on the surface of the films as shown in Fig. 40 c). If the whiskers were formed by the stresses in underlying metal as generally believed[22], their cause might not be the volume misfit among oxide and metal because the film is too thin to affect the stress, but be the agglomeration of hydrogen as will be written later. The formation of α-Al_2O_3 at 350°C is deviated from the equilibrium phase diagram[23] in Fig. 41.

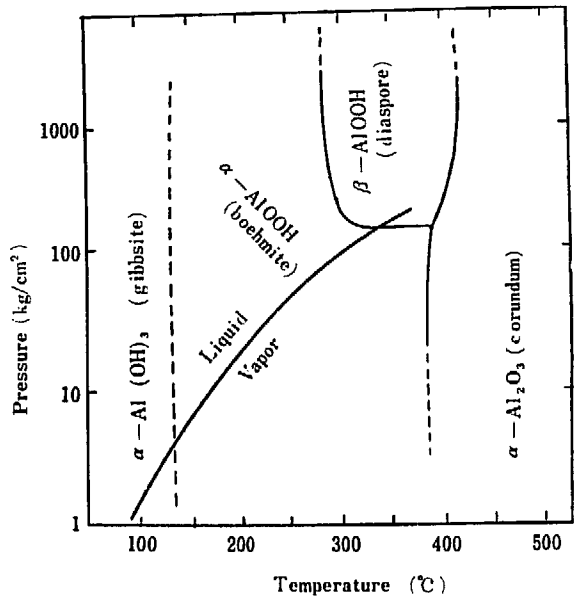

Fig. 41 Equilibrium diagram for the system Al_2O_3-H_2O (Ervin, Osborn)

The agglomeration of hydrogen at grain boundaries: The optical micrographs of the cross section of the specimens exposed at 400°C are shown in Fig. 42 a), b) and Fig. 43 a), b); there appeared at grain boundaries a number of pores which increased in size and number with increasing time and pressure, especially just before the initiation of the penetration attack. Considering the extremely small amount of oxidation this large absorption and agglomeration increased considerably as shown in Fig. 45 which also shows the acceleration of the reaction by the destructive action of hydrogen. The pores were made larger by annealing for one hour at 500°C.

DRALEY *et al.*[21] reported that the hydrogen was absorbed mainly at the initial stage of exposure. However, it is not clear whether or not the hydrogen was absorbed continuously after the film formation, as the amount of the reaction was too

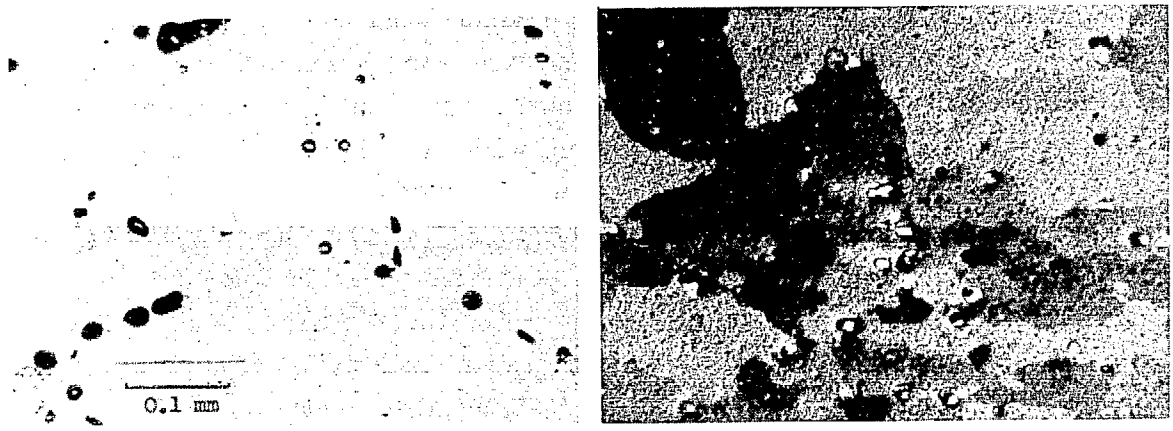

a) Ordinary light b) Polarized light

Fig. 42 Microphotographs of the cross section of 99% Al exposed for 20 hours to superheated steam at 400°C, 20 kg/cm² (×120)

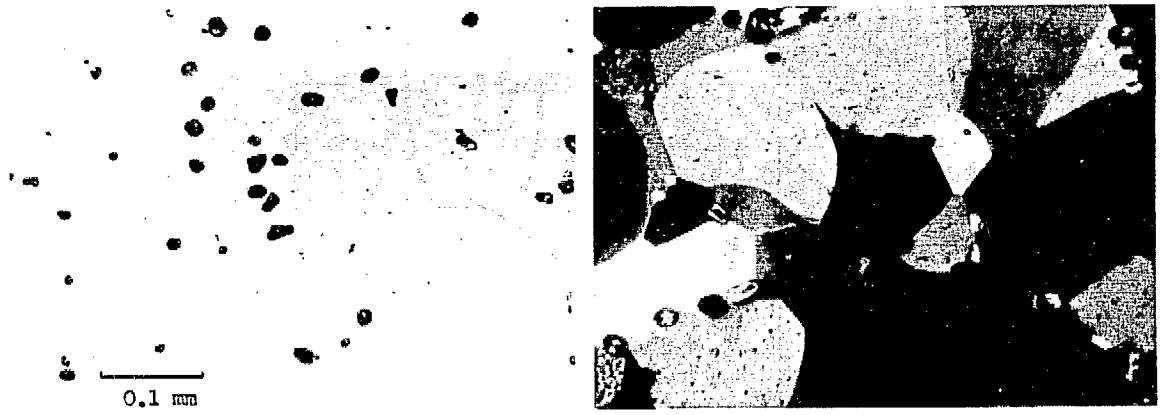

a) Ordinary light b) Polarized light

Fig. 43 Microphotographs of the cross section of 99.99% Al exposed for 20 hours to superheated steam at 400°C, 20 kg/cm (×120)

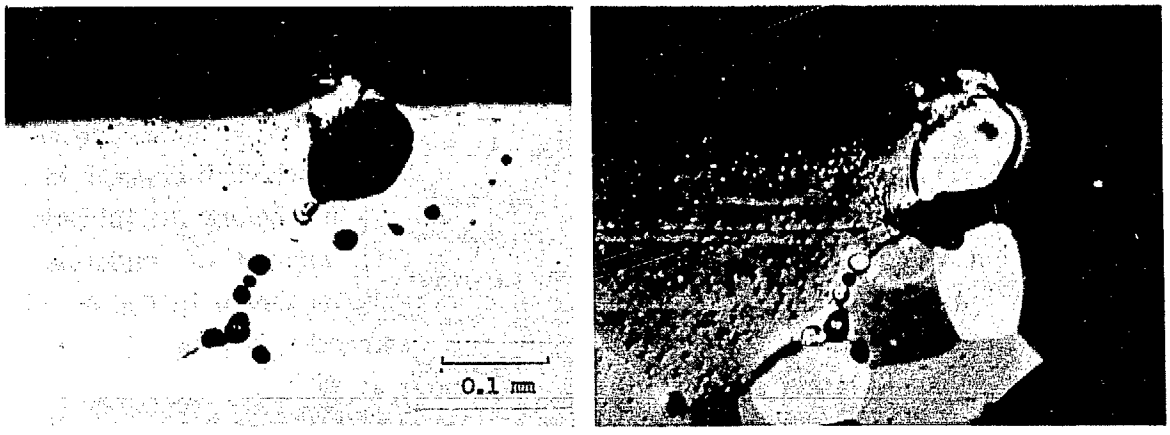

a) Ordinary light b) Polarized light

Fig. 44 Blister formation at the grain boundary beneath the surface due to the agglomeration of hydrogen (×120)

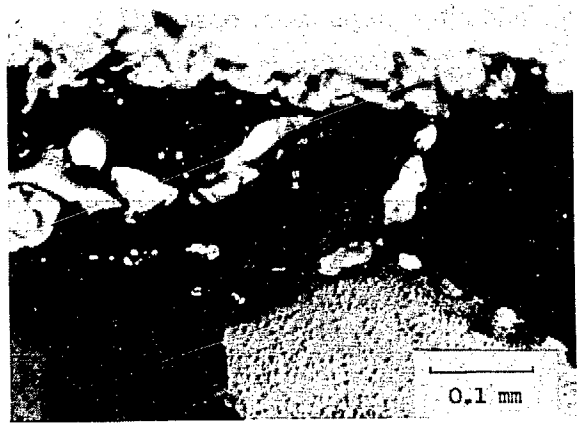

Fig. 45 Intergranular penetration of hydrogen at the oxide-metal interface (×120)

small to be measured. And if the attack was induced only by the hydrogen initially absorbed, the induction time would correspond to the time required for its migration to the grain boundary. There was not observed the intergranular attack as observed at lower temperatures but formed chained micro-pits along the subgrain boundaries of the metal as seen in the electron micrograph in Fig. 46.

The defect portions such as the network of the substructure and grain boundary will serve as the inlet paths for atomic hydrogen since the solid solubility of hydrogen will increase at higher temperatures.

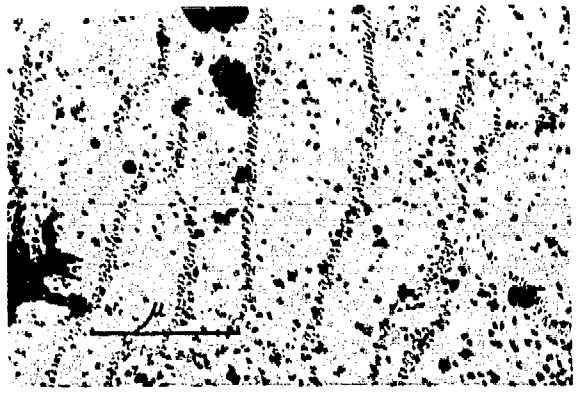

Fig. 46 Transmission electron micrograph of surface film formed on 99% Al by exposure in super heated steam at 400°C, 18 kg/cm². Micro-pits are observed along the substructure net-work

c) Hydrothermal treatment of α-Al_2O_3 formed in penetration attack

It has been observed a marked difference between higher and lower temperature ranges in corrosion behavior. Thus the test, exposing anhydrous α-Al_2O_3 to the steam at 300°C, was attempted to examine the hydration process.

Two kinds of oxide power, formed in steam at 500°C, were compared their hydration process in the steam at 300°C, 90 kg/cm². From the results illustrated in

TABLE 10 and Fig. 47 the following steps were observed;

$$\alpha\text{-}Al_2O_3 \rightarrow \beta\text{-AlOOH (diaspore)} \rightarrow \alpha\text{-AlOOH (boehmite)}$$

TABLE 10 Intensities of X-ray diffraction spectra from the bulk α-Al_2O_3 hydrothermally treated in steam at 300°C, 90 kg/cm²

Test sample	Exposure (hr)	Transition products			
		Diaspore (β-AlOOH)		Boehmite (α-AlOOH)	
		d(Å)·(hkl) 3.99(110)	2.131(121)	1.860(501)	1.850(020)
99% Al	3	8	weak	0	0
	11	124	60	weak	weak
	20	6	weak	115	82
99.99% Al	3	186	66	8	7
	11	250	102	12	10
	20	30	14	154	111

Cu, K-α relative intensity (C. P. S.)

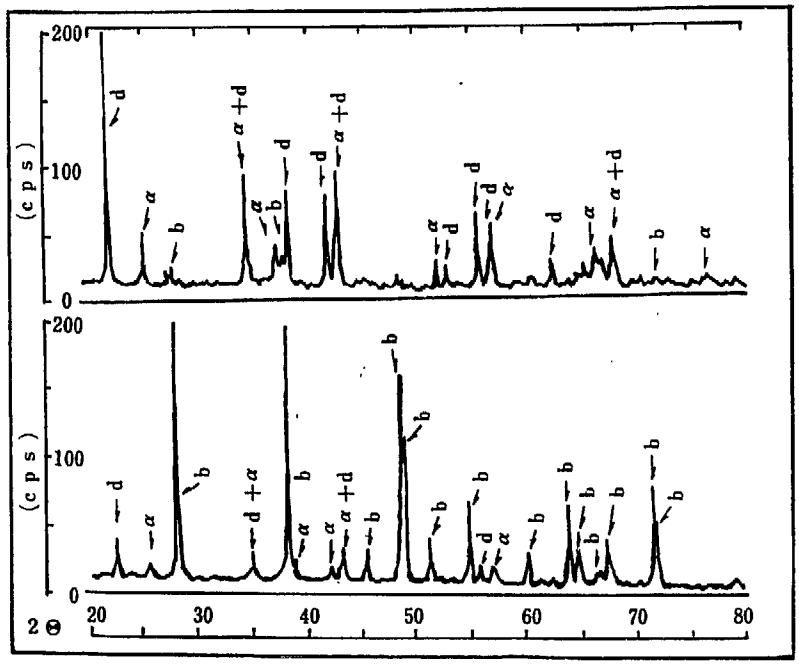

(a) α —Al_2O_3 treated for 3 hours, diaspore is the most dominant

(b) α —Al_2O_3 treated for 20 hours, boehmite is the most dominant

α ·····α—Al_2O_3, d ·····diaspore b ·····boehmite

Fig. 47 X-ray diffractions of oxide powder hydrothermally treated in steam at 300°C, 90 kg/cm² (99.99% Al)

The oxide formed on 99.99% aluminum is hydrated much faster than 99% one so that the hydration, as far as the present experiment concerns, is largely influenced by the impurities in the material. If the hydration reaction itself is sufficiently rapid comparing to the diffusion of hydrating species through the outer hydrated layer or to the recrystallization of the hydrated oxide, the latter would be the controlling step so that the present experiment would be an estimation for corrosion consideration. The effect of impurities on the diffusion of deutron in boehmite crystal is also observed by other workers[24].

2.3 Conclusion

The corrosion of aluminum in water and steam at boehmite-forming temperatures was experimentally interpreted by the destructive action of hydrogen and inward-hydration of the surface oxide which in turn is controlled by the migration of some hydrogen-bearing carries and/or the recrystallization of hydrated oxide. Several additional phenomena were also examined through various experiments and were discussed.

At higher temperatures, where anhydrous oxide was formed, the corrosion behavior in superheated steam was much different from that of lower temperatures. However the same relation was derived in the pressure dependence of corrosion rate between them.

The mechanism of the penetration attack at higher temperatures was studied by the observation of the hydrogen agglomeration at grain boundary and penetration-induction time.

REFERENCES

1) Japan Institute of Light Metals: "Studies on Corrosion of Aluminum Alloy for Water Cooled Reactor" (1960)
2) R. K. HART: *Trans. Faraday Soc.*, **53**, 1020 (1957)
3) J. E. DRALEY: TID-7587 165
4) N. CABRERA and N. F. MOTT: *Rept. Prog. Phys.*, **12**, 163 (1948-49)
5) K. VIDEM: *J. Nucl. Mat.* **2**, 145 (1959)
6) K. SAKAMOTO: *J. Japan Ceramic Soc.* (in Japanese) **67**, c 114 (1959)
7) E. DELTOMBE and M. POURBAIX: *Corrosion* **14**, 496 t (1958)
8) M. S. HUNTER and P. FOWLE: *J. Electochem. Soc.*, **101**, 481 (1954)
9) S. R. HATCHER and H. K. RAE: "Formation and Control of Turbidity in Aluminum-Water Reactor Systems" AECL-report
10) K. MOTOJIMA: *J. Japan Chem. Soc.*, **76**, 903 (1995)
11) M. J. PRYOR and D. S. KEIR: *J. Electrochem. Soc.*, **104**, 370 (1955)
12) M. KAWASAKI, S. NOMURA and T. KONDO: *J. Japan Inst. Met.*, **25**, 76 (1961)

13) J. E. DRALEY and W. E. RUTHER: ANL-5658, April (1957)
14) D. ALTEPOHL: *Z. Metallk.*, **48**, 306 (1957)
15) M. KAWASAKI, T. KONDO and S. NOMURA: *J. Japan Inst. Met.*, **25**, 80 (1961)
16) T. KONDO, C. AKUTSU and M. KAWASAKI: *Trans. Japan Inst. Met.*, **3**, 1 (1962)
17) R. L. DILLON and V. H. TROUTNER: HW-31849, Sep. (1957)
18) C. WAGNER: *Z. Phys. Chem.*, **22**, 212 (1933)
19) N. J. M. WILKINS and J. N. WANKLYN: *J. Inst. Met.*, 88, 134 (1959-60)
20) M. S. HUNTER and P. FOWLE: *J. Electrochem. Soc.*, **108**, 139 (1961)
21) J. E. DRALEY, W. E. RUTHER and S. GREENBERG: ANL-6207, Apr. (1961)
22) F. C. FRANK: *Phil. Mag.*, **44**, 854 (1953)
23) G. ERVIN and E. F. OSBORN: *J. Geol.*, **59**, 381 (1951)
24) S. MORI, J. E. DRALEY and R. B. BERNSTEIN: ANL-5889, Add. Apr. (1961)